MASTER

A discontinuous Galerkin method for multi-dimensional moment systems

Wolf, M.C.W.

Award date:
2015

A Discontinuous Galerkin Method for Multi-dimensional Moment Systems

M.C.W. Wolf

September 28, 2015

Author:
M.C.W. Wolf

Supervisors:
Prof.dr.ir. E.H. van Brummelen
Ir. M.R.A. Abdel Malik

Technische Universiteit **Eindhoven** University of Technology

Department of Mechanical Engineering

Thermo Fluids Engineering
Multiscale Engineering Fluid Dynamics

Department of Mathematics and Computer Science

Industrial and Applied Mathematics
Computational Science and Engineering

Abstract

This Msc project is concerned with the numerical approximation of multi-dimensional moment systems and is an extention of the work of M.R.A. Abdel Malik [19]. The classical fluid descriptions such as the Euler equations and Navier-Stokes equations lose their validity in rarefied regimes. Those regimes are characterized by Knudsen numbers (Kn) between $0.01 \lesssim \text{Kn} \lesssim 10$. A kinetic model for which the validity extends into the rarefied regime is the Boltzmann equation (BE). This model also recovers the Euler-equations and Navier-Stokes equations when $Kn \to 0$. Constructing numerical approximations to the BE is a daunting challenge because of its high dimensional setting.

The method of moments [14, 18] is a promising alternative which tries to simplify the kinetic model. It creates a hierarchy of approximations to the BE, such that each member of the hierarchy corresponds to a hyperbolic system of partial differential equations. These equations generate balance laws for velocity moments of a kinetic density. The system retain structural features of the BE such as the celebrated Boltzmann's H-Theorem, i.e. solutions to the moment system are entropy dissipative.

Using the method of moments leads to the moment closure problem which will use entropy-based moment closure techniques. Problems pertaining to the analytical formulation and computational implementation of the moment closure system were investigated in [19]. The author considered a new class of moment closure approximation for the BE in 1 spatial dimension. In this class, the velocity moments of exponentials, containing velocity polynomials, can numerically be approximated. He also showed that the system of partial differential equations using this new class still retains the fundamental properties of the BE.

The current work will consider the extension of this new class to multiple dimensions. In addition, a Discontinuous Galerkin (DG) finite element method is developed to approximate the moment systems in the velocity dependence. Particular consideration is given to the numerical flux in the DG method.

This report presents both the theoretically analysis of the moment system and the DG method as well as numerical simulations.

Keywords: Boltzmann equation; Discontinuous Galerkin method; Numerical-flux; Moment closure; Multi-dimensional; Hyperbolic systems; Kinetic theory; BGK-operator

Contents

List of Symbols

$\boldsymbol{\xi}$	Molecular velocity
$\boldsymbol{\lambda}$	Vector of closure coefficients
$\boldsymbol{\mathcal{J}}$	Flux vector
$\boldsymbol{\mathcal{Q}}$	Collision vector
$\widetilde{\boldsymbol{\mathcal{J}}}$	Numerical flux vector
$\boldsymbol{a}$	Acceleration vector
$\boldsymbol{m}$	Vector of velocity weights
$\boldsymbol{U}, \boldsymbol{\rho}$	Realizable values, velocity moment vector of f corresponding to the macroscopic properties
$\boldsymbol{x}$	Position vector
λ	mean free path
$\mathcal{M}$	Maxwellian distribution function
ν	Relaxation frequency
ρ	Mass density
τ	Relaxation time $(1/\nu)$
τ_{ij}	Deviatoric stress tensor
Θ	Rescaled temperature, $= kT/m = RT/M$
θ	Dimension of the vector $\mathbf{m(v)}$
$\tilde{n}$	Number of mole of gas
e	Internal energy per unit mass
f	Velocity distribution function

k	Boltzmann's constant, $= 1.3806488 \times 10^{23} JK^{-1}$
Kn	Knudsen number, $= \lambda / L$
L	Characteristic length of the flow field
M	Molecular weight, kg/mol
m	Molecular mass, g
n	Number density
P	Isotropic pressure
p_{ij}	Anisotropic pressure tensor
Pr	Prandtl number
q_i	Heat flux
R	Gas constant $8.314462175 JK^{-1} mol^{-1}$
T	Temperature
t	Time
$\mathbf{u}$	Bulk velocity of the gas, mean molecular velocity

Chapter 1

Introduction

The modeling of gases can be considered either from a macroscopic or microscopic scale. Observing it from a macroscopic scale, the gas will be treated as a continuous medium and the desciption is modeled by the fluid variables; mass density, fluid velocity and temperature. The evolution of these variables are governed by the (compressible) Euler or Navier-Stokes-Fourier equations. However, the choice of considering it from a macroscopic or microscopic scale depends on the dimensionless Knudsen number, defined as the ratio of the mean free path λ to a typically macroscopic length scale L. The mean free path is the averaged distance a particle travels between collisions. The Knudsen number can be used to define several flow regimes which are,

- Kn $\lesssim 0.01$: The hydrodynamic regime, which can be wel described by the Euler and Navier-Stokes equations
- $0.01 \lesssim$ Kn $\lesssim 10$: Transition regime, both the Euler and Navier-Stokes fail. The gas needs to be describe by e.g. Boltzmann equation or by extended macroscopic models
- Kn $\gtrsim 10$: Free molecular flow, the amount of collisions between particles is lower than the collisions between particles and wall. Therefore, the latter dominates which makes particle models like the Direct Simulation Monte Carlo (DSMC) method more suitable.

For modeling gases in the transition regime, called rarefied gases, none of the continuum models are valid. The gas needs to be considered from a microscopic scale in which the evolution will be describe with the Boltzmann equation. Since the Boltzmann equation can also be used for Knudsen numbers which are lower than 0.01 or greater than 10, the modeling of gases from a microscopic scale seems to be a more fruitful way. However, the Euler and Navier-Stokes equations will be recovered from the Boltzmann equations as $Kn \to 0$. At the microscopic scale, the gas will be treated as a collection of particles characterized by their velocity and position.

For small Knudsen numbers i.e. Kn$\ll 1$, the velocity distribution of the particles will approach a local equilibrium. These can be parametrized by the aforementioned macroscopic fluid variables which are, mass density, fluid velocity and temperature. As mentioned, the evolution of these variables are governed by the (compressible) Euler equations, which approximate the velocity distribution by a local equilibrium or by the Navier-Stokes-Fourier

equations, which acount for small deviations of the velocity distribution from a local equilibrium. As the Knudsen number increases, the basic assumption of the fluid dynamics (which is $\lambda << L$) breaks down and microscale effects or effects of gas rarefaction become important to desscribe the gas flow. Processes in which this occurs are [27] for instance,

- High altitude flight, where gas pressure and density are very low. The mean free path becomes so large that the Knudsen number cannot be considered to be small even for the macroscopic dimensions of the body of a space craft
- Micro channel flow or flow in porous media, the relevant macroscopic length scale L becomes comparable to the mean free path. The Knudsen number becomes significant

1.1 Content and structure of this thesis

Since this thesis is primarily devoted to obtaining numerical results for the Boltzmann equation in one and two spatial dimensions, the theory of the Boltzmann equation presented in this thesis is a recapitulation of the theory which can be found in Levermore [18] and Abdel Malik [19].

Chapter 2 is a review of the concept of kinetic theory of gases. It introduces the velocity distribution function f for which the evolution is given by the Boltzmann equation. In general, the macroscopic properties are the most interested. Therefore, the relation of the distribution function and the macroscopic properties will also be given.

Chapter 3 presents the Boltzmann equation. The first section presents the Boltzmann equation itself as well as its three fundamental properties. Next, the notion of the method of moment is introduced which is then applied to the Boltzmann equation. With the moment closure problem presented, section 3 considers the closure procedure. This section is a summary of the chapter 2 and partially chapter 3 of Abdel Malik [19].

Chapter 4 considers the right hand side of the Boltzmann equation which is the collision integral. Because of its complicated structure, the evaluation and approximation is a difficult task. The well-known BGK collision model will be introduced which makes the numerical approximation of the collision intergal tractable. Since every collision model needs to retain the three fundamental properties of the Boltzmann equation, it will be shown that this is the case for the BGK model.

Chapter 5 treats the numerical scheme which is the Discontinuous Galerkin finite element method. Starting with the strong formulation of the closed moment system in order to obtain the weak formulation after this. Because of the DG method, a numerical flux needs to be considered which will be derived. In the last two sections, different boundary conditions are presented and the velocity space integrations needed for the numerical inplementation are shown.

Finally, chapter 6 contains the numerical simulations of the Boltzmann equation. This contains the results for different number of moment systems as well as convergence tests using mesh refinements.

Chapter 2

Concept of Kinetic Theory

This chapter is concerned with a short introduction of the kinetic theory of gases. After the introduction, the concept of the velocity distribution function f will be treated. Herein, relations to the number of particles or number density will be given. The last section describe the relation between this distribution function and the macroscopic properties. To be more precise, the velocity moments of the distribution function corresponds to different macroscopic properties. For more detailed introductions on kinetic theory and the Boltzmann equation see [7, 9, 10, 31].

2.1 Introduction

In kinetic theory, gas is considered from a microscopic level of individual molecules which are in constant motion. The motion of the molecules will be regarded as chaotic and are continuously colliding with each other or with any present surface. This is where the gas differs with more ordered states like liquid or solid. Assuming that the laws of interaction between molecules are known and that the molecules obeying the laws of classical mechanics, it would in principle be possible to follow each molecule in time given some initial condition which are not known of course. However, only for very "small" number of molecules this would be calculable. Given the fact that there are about 2.7×10^{19} molecules in a cubic centimeter of a gas at atmospheric pressure and a temperature of 0 °C, this would be a difficult task to complete. Fortunately, there is no need for all the detailed information. Knowing the velocity and position of all the single particles does not give any usable information. The only useful information are the macroscopic quantities such as pressure, temperature, stress and density. Furthermore, only the change in those quantitites can be observed [8].
Another thing to notice is the behavior of the particles for different initial conditions: A slightly different initial condition will give different velocities and positions of the particles. The point is, one should consider the evolution not of one system but of a sequence of identical systems in which the initial data differs from each other within a prescribed error. Thus considering only the behavior of many systems will give a reliable and useful result, therefore a recourse to statistic should be made.
Since we are talking about probabilities, the particles will not have a definite position and velocity but different probabilities of having different positions and velocities. Probability density functions for the gas, $F(t, \mathbf{x}, \boldsymbol{\xi})$, are defined in phase space and specify the probability

of finding particles at a given location x_i and time t, having a particular gas velocity, ξ_i. The phase space is a multi-dimensional space formed by the combination of the physical space and the velocity space. Macroscopic quantities of the gas are then obtained by taking appropriate velocity moments of $F(t, \mathbf{x}, \boldsymbol{\xi})$.

2.2 The velocity distribution function

As mentioned earlier, a gas would be completely described if its position, velocity and internal state of each particle would be known. However, because of the large number of particles, this would be an unthinkable task. Therefore, the statistical description in terms of probability distribution are needed. To avoid confusion with different terminologies, a general review about the distributions will be given.

Consider a gas that is homogeneous in physical space and contains N identical particles. A particle will have a velocity $\boldsymbol{\xi}$ with components ξ_1, ξ_2 and ξ_3. Similar to the physical space, these components will define a velocity space in which each particle can be represented. For simplicity, consider the one dimensional velocity space (which is a line) with component ξ. If all the velocities of the particles at a certain time instant t and point x are known, then each velocity could be plotted on this line as a point. This will create a distribution of the velocities on the one-dimensional velocity space. This distribution is called the *probability distribution function*. Because the variable ξ is continuous, $-\infty \leq \xi \leq \infty$, it is also called the *probability density function* or the *velocity distribution function* since it is a distribution in velocity space. However, given some distribution function, it defines the probability of having particles with velocity in the range $\xi + d\xi$. Thus it is defined for a velocity range and not for a particular velocity.

The velocity distribution function solely depends on $\boldsymbol{\xi}$ and is normalized, which implies,

$$\int_{\boldsymbol{\xi} \in \mathbb{R}^D} \tilde{f}(\boldsymbol{\xi}) d\boldsymbol{\xi} = 1$$

Since we assumed that the particles are identical, $f(\boldsymbol{\xi})$ is called the single-particle velocity distribution function or just single-particle distribution function. The number of particles which possess a velocity in the range $d\boldsymbol{\xi}$ is,

$$dN = N\tilde{f}(\boldsymbol{\xi}) d\boldsymbol{\xi}$$

Dividing both side by the total volume V gives the number of particles with velocity in the range $d\boldsymbol{\xi}$ per unit volume,

$$dn = n\tilde{f}(\boldsymbol{\xi}) d\boldsymbol{\xi}$$

with n the number density. Clearly, if the distribution of the particles through space and time is non-uniform then $n := n(t, \boldsymbol{x})$. To conclude, the number of particle in the physical range $d\boldsymbol{x}$ with velocities in the range $d\boldsymbol{\xi}$ is,

$$dN = n(t, \boldsymbol{x})\tilde{f}(\boldsymbol{\xi}) d\boldsymbol{\xi} d\boldsymbol{x}$$

We define $\mathcal{F}(t, \boldsymbol{x}, \boldsymbol{\xi}) = n(t, \boldsymbol{x})\tilde{f}(t, \boldsymbol{x}, \boldsymbol{\xi})$ as the single-particle distribution function which is nonnegative and defined over a single-particle space $\Omega \times \mathbb{R}^D$.

2.3 The macrosopic variables

In the previous section, the concept of the velocity distribution function $\tilde{f}$ has been introduced. If the velocity distribution function of the gas is known, then all the macroscopic properties of the gas are known. Those macroscopic quantities are obtained by finding the moments of $\tilde{f}$. The moments are defined as multiplying $\tilde{f}$ by an appropriate velocity-dependent function and integrating over the entire velocity space.

According to the definition of $\mathcal{F}(t, \boldsymbol{x}, \boldsymbol{\xi})$ in the previous section, $\mathcal{F}(t, \boldsymbol{x}, \boldsymbol{\xi}) d\boldsymbol{\xi} d\boldsymbol{x}$ is the number of particles at time t in the physical space element $d\boldsymbol{x}$ near $\boldsymbol{x}$ with velocities in the velocity space $d\boldsymbol{\xi}$ near $\boldsymbol{\xi}$. Integrating $\mathcal{F}$ over the entire velocity space $\boldsymbol{\xi}$, one obtains the total number of particles per unit volume which is the number density of the particles.
Before introducing the macroscopic properties, let m be the molecular mass. By multiplying $\mathcal{F}$ with the mass m, define $f(t, \boldsymbol{x}, \boldsymbol{\xi}) = m\mathcal{F}(t, \boldsymbol{x}, \boldsymbol{\xi})$ as the one-particle marginal distribution function which will be called the (phase-space) *density*. The reason for doing this will become obvious by the next definitions.

The macroscopic properties will be defined by using components, i.e. the subscript i, j with $i, j = 1, 2, 3$ will denote the corresponding variable in x, y, z spatial directions. The density $\rho(t, \boldsymbol{x})$ and the mass flow $\rho \boldsymbol{u}(t, \boldsymbol{x})$ in the physical space are,

$$\rho = \int_{\boldsymbol{\xi} \in \mathbb{R}^D} f d\boldsymbol{\xi}, \qquad \rho u_j = \int_{\boldsymbol{\xi} \in \mathbb{R}^D} \xi_j f d\boldsymbol{\xi}$$

The momentum flow and energy per unit volume are,

$$\rho u_i u_j + p_{ij} = \int_{\boldsymbol{\xi} \in \mathbb{R}^D} \xi_i \xi_j f d\boldsymbol{\xi}, \qquad \frac{1}{2}\rho |\boldsymbol{u}|^2 + \rho e = \int_{\boldsymbol{\xi} \in \mathbb{R}^D} \frac{1}{2} |\boldsymbol{\xi}|^2 d\boldsymbol{\xi} \tag{2.1}$$

and the energy flow is,

$$\frac{1}{2}\rho |\boldsymbol{u}|^2 u_i + \rho e u_i + \sum_{j=1}^{3} u_j p_{ij} + q_i = \frac{1}{2} \int_{\boldsymbol{\xi} \in \mathbb{R}^D} |\boldsymbol{\xi}|^2 \xi_i d\boldsymbol{\xi} \tag{2.2}$$

with q_i the heat flux and "e" is the internal energy per unit mass which are defined as,

$$q_i = \frac{1}{2} \int_{\boldsymbol{\xi} \in \mathbb{R}^D} |\boldsymbol{\xi} - \boldsymbol{u}|^2 (\xi_j - u_j) f d\boldsymbol{\xi}, \qquad \rho e = \frac{1}{2} \int_{\boldsymbol{\xi} \in \mathbb{R}^D} |\boldsymbol{\xi} - \boldsymbol{u}|^2 f d\boldsymbol{\xi}$$

The pressure tensor p_{ij}, which plays the role of the stress tensor, is defined by,

$$p_{ij} = \int_{\boldsymbol{\xi} \in \mathbb{R}^D} (\xi_i - u_i)(\xi_j - u_j) f d\boldsymbol{\xi}$$

It is related to the deviatoric stress tensor τ_{ij} via $p_{ij} = \delta_{ij} P - \tau_{ij}$, with $P = p_{ii}/D$ the isotropic pressure. Observe that ρe is equal to $\frac{1}{2}$ times the trace of the matrix p_{ij}. Furthermore, the diagonal components τ_{ii} of the symmetric stress tensor are zero for a monatomic gas.

Using the ideal gas law $PV = \tilde{n}RT$, the pressure P can be written as, $P = \tilde{n}RT/V = (\tilde{n}M/V) \times (RT/M) = \rho\Theta$. The equations in (2.1) can be rewritten as,

$$\rho u_i u_j + \delta_{ij}\rho\Theta - \tau_{ij} = \int_{\boldsymbol{\xi}\in\mathbb{R}^D} \xi_i \xi_j f d\boldsymbol{\xi}, \qquad \frac{1}{2}\rho|\boldsymbol{u}|^2 + \frac{D}{2}\rho\Theta = \int_{\boldsymbol{\xi}\in\mathbb{R}^D} \frac{1}{2}|\boldsymbol{\xi}|^2 d\boldsymbol{\xi}$$

Also the energy flow (2.2) can be rewritten as,

$$\frac{1}{2}\rho|\boldsymbol{u}|^2 u_i + \frac{D+2}{2}\rho\Theta u_i - \sum_{j=1}^{3} \tau_{ij}u_j + q_i = \frac{1}{2}\int_{\boldsymbol{\xi}\in\mathbb{R}^D} |\boldsymbol{\xi}|^2 \xi_i d\boldsymbol{\xi}$$

with D the spatial dimension.

In general, moments of arbitrarily high order can be taken. Since the macroscopic properties can be found at relatively low order of moments, the physical meaning of the higher order moments become less obvious.

Chapter 3

The Boltzmann Equation

3.1 Introduction

In the previous chapter, the concept of the velocity distribution function has been introduced as well as some macroscopic quantities. Those quantities have been expressed through the velocity distribution function by taking their moments with respect to the velocity $\boldsymbol{\xi}$. This function give a statistical description of the gas on the molecular level. The question is, how to find this velocity distribution function. The answer is given by the *Boltzmann* equation which describes the time evolution of the velocity distribution of the gas. The complete Boltzmann equation is given by,

$$\frac{\partial f}{\partial t} + \boldsymbol{\xi} \cdot \frac{\partial f}{\partial \mathbf{x}} + \boldsymbol{a} \cdot \frac{\partial f}{\partial \boldsymbol{\xi}} = \mathscr{C}(f) \tag{3.1}$$

Here, $\mathbf{a}$ is the particle acceleration due to external forces like gravity and is taken to be zero in this thesis and $\boldsymbol{\xi}$ is the velocity of the molecule. The term on the right hand side represents the collision term which describes the effect of the collisions between molecules on the distribution function.

The phase-space density $f(t, \mathbf{x}, \boldsymbol{\xi})$ is nonnegative and its evolution is described over a single particle phase space $\Omega \times \mathbb{R}^D$. The collision operator $f \to \mathscr{C}(f)$ acts only on the $\boldsymbol{\xi}$ dependence of f locally at each $(t, \mathbf{x})$. A fixed domain $\Omega \subset \mathbb{R}^D$ will be considered in which the gas is composed of a single species of identical particles (a monatomic gas).

Introducing the following notation, the integral of any scalar or vector-valued measurable function over the D-dimensional Lebesgue measure $d^D_{\boldsymbol{\xi}}$ will be denoted by,

$$\langle f \rangle = \int_{\boldsymbol{\xi}} f(\boldsymbol{\xi}) d^D_{\boldsymbol{\xi}}$$

It will be assumed that all functions considered within this thesis are Lebesgue measurable in all variables.

More information about the derivations of the Boltzmann equation and the collision term can be found in e.g. Shen [11], Cercignani [7, 8] and Bird [4].

3.1.1 Properties of the collision operator

The Boltzmann collision operator $\mathscr{C}$ has three fundamental properties. It is assumed that the operator is defined over the domain $\mathscr{D}(\mathscr{C})$ that is contained within the cone of nonnegative functions of $\boldsymbol{\xi}$. Its properties are [18, 19]:

1. ***Conservation of Mass, Momentum and Energy***
   The operator $\mathscr{C}$ is assumed to have $\gamma \in \{1, \xi_1, \xi_2, \xi_3, |\boldsymbol{\xi}|^2\}$ as locally conserved quantities: i.e.
   $$\Big\langle \gamma \mathscr{C}(f) \Big\rangle = 0 \qquad \forall f \in \mathscr{D}(\mathscr{C}) \tag{3.2}$$
   The above relations represent the laws of mass, momentum and energy conservation during collision. It is assumed that there are no further conservation laws and that every locally conserved quantity is a linear combination of the above relations, so that for any $g = g(v)$ the following statements are equivalent:
   $$(i) \qquad \Big\langle g \mathscr{C}(f) \Big\rangle = 0 \qquad \forall f \in \mathscr{D}(\mathscr{C}) \tag{3.3}$$
   $$(ii) \qquad g \in \mathbb{E} \equiv \text{span}\{1, \xi_1, \xi_2, ..., \xi_d, |\boldsymbol{\xi}|^2\} \tag{3.4}$$

2. ***Dissipation of entropy: H-theorem***
   The operator $\mathscr{C}$ is assumed to satisfy the local dissipation relation,
   $$\Big\langle \ln f \mathscr{C}(f) \Big\rangle \leq 0 \qquad \forall f \in \mathscr{D}(\mathscr{C}) \tag{3.5}$$
   The local equilibria of $\mathscr{C}$ are assumed to be characterized by the vanishing of the local entropy dissipation rate and to be given by the class of Maxwellian densities which have the form,
   $$f = \mathcal{M}(\rho, \mathbf{u}, \Theta) = \frac{\rho}{(2\pi\Theta)^{D/2}} \exp\Big(- \frac{|\boldsymbol{\xi} - \mathbf{u}|^2}{2\Theta} \Big) \tag{3.6}$$
   for some $(\rho, \mathbf{u}, \Theta) \in \mathbb{R}_+ \times \mathbb{R}^D \times \mathbb{R}_+$. More precisely, for every $f \in \mathscr{D}(\mathscr{C})$ the following statements are assumed to be equivalent,
   $$(i) \qquad \Big\langle \ln f \mathscr{C}(f) \Big\rangle = 0 \tag{3.7}$$
   $$(ii) \qquad \mathscr{C}(f) = 0 \tag{3.8}$$
   $$(iii) \qquad f \text{ is a Maxwellian density given by 3.6} \tag{3.9}$$

3. ***Galilean invariance***
   The operator $\mathscr{C}$ is assumed to commute with translational and orthogonal transformations. Specifically, given $f = f(\boldsymbol{\xi})$, then for every vector $\boldsymbol{u} \in \mathbb{R}^D$ and for every orthogonal matrix $O \in \mathbb{R}^{D \times D}$ define transformed functions $\mathscr{T}_u f$ and $\mathscr{T}_o f$ by,
   $$(i) \qquad \mathscr{T}_u f = \mathscr{T}_u f(\boldsymbol{\xi}) \equiv f(\boldsymbol{u} - \boldsymbol{\xi}) \tag{3.10}$$
   $$(ii) \qquad \mathscr{T}_o f = \mathscr{T}_o f(\boldsymbol{\xi}) \equiv f(O^T \boldsymbol{\xi}) \tag{3.11}$$
   The kinetic equation 3.1 formally retains Galilean invariance, i.e. whenever $f(t, \boldsymbol{x}, \boldsymbol{\xi})$ satisfy 3.1 so do the actions of the Galilean group on f. This implies the Galilean invariance of the microscopic collisional dynamics.

3.2 Moment system

At first sight, solving the Boltzmann equation (3.1) to obtain the phase-space density $f(t, \mathbf{x}, \boldsymbol{\xi})$ would be the best choice. However, the amount of information obtained from the phase-space density f is maybe not so usefull. In most practicle applications, the quantities that are measurable and interesting are the macroscopic quantities such as the density ρ, velocity $\mathbf{u}$ and rescaled temperature Θ. As we have seen in the previous chapter, those quantities are obtained through the multiplication of the velocity distribution function f by either $\{1, \boldsymbol{\xi}, |\boldsymbol{\xi}|^2\}$ and integration over the velocity space. These averages are referred to as the moments of the velocity distribution function f. So rather than solving equation (3.1), it is more convenient to resolve moments of the Boltzmann equation. Those moments of the Boltzmann equation govern the evolution of a finite set of velocity moments of f. This approach reduces the complexity of (3.1) since it replaces the velocity dependence of f by a finite number of parameters [15, 19, 21].

The derivation of the monent equations begins with the choice of a linear subspace $\mathbb{M}$ of functions of $\boldsymbol{\xi}$, usually polynomials of $\boldsymbol{\xi}$. Denote by θ the dimension of this space and $\{m_i = m_i(\boldsymbol{\xi})\}_{i=1}^{\theta}$ a basis. Also denote the column θ - vector of these basis elements by $\mathbf{m} = \mathbf{m}(\boldsymbol{\xi})$ such that every $m \in \mathbb{M}$ has a unique representation in the form $m(\boldsymbol{\xi}) = \boldsymbol{\alpha}^T \mathbf{m}(\boldsymbol{\xi})$ for some $\boldsymbol{\alpha} \in \mathbb{R}^\theta$. Consider the space of phase-space density distributions given by,

$$\mathcal{F} := \{f \in \mathbb{L}^1(\mathbb{R}^D) : f \gneq 0 \text{ and } (m_i f) \in \mathbb{L}^1(\mathbb{R}^D) \quad \forall i \in \{1, 2, ..., \theta\}\}$$

Next taking the moments of the kinetic equation (3.1) over the vector $\mathbf{m}(\boldsymbol{\xi})$,

$$\partial_t \langle \mathbf{m} f \rangle + \partial_{x_j} \langle \xi_j \mathbf{m} f \rangle = \langle \mathbf{m} \mathscr{C}(f) \rangle \tag{3.12}$$

Hence, the moment equations (3.12) is a system of partial differential equations. It should be mentioned that it is not known whether the quantities appearing in this equation are well defined for every solution f. However, recent work has shown that this is the case for space-homogeneous solutions [12]. At this point, it will be assumed that the quantities are well defined.

It is clear that the moment system (3.12) does not represent a closed system: There are more unknowns that equations. The flux term $\langle \xi_j \mathbf{m} f \rangle$ includes moments of one order higher in ξ_j than the density $\langle \mathbf{m} f \rangle$. Thus the time evolution of every moment is dependent on a moment of one order higher in ξ_j. In order to obtain a closed system of moment equations, the flux terms $\langle \xi_j \mathbf{m} f \rangle$ and the collision terms $\langle \boldsymbol{m} \mathscr{C}(f) \rangle$ needs to be expressed in terms of the density $\langle \mathbf{m} f \rangle$. This can be achieved by finding a relation between the moments and the distribution function. This process is called the moment closure problem.

3.2.1 Moment closure

To obtain a closed system of the moment equations, a constitutive relation is needed which expresses the densities $\langle \mathbf{m} f \rangle$, fluxes $\langle \xi_j \mathbf{m} f \rangle$ and collisions terms $\langle \boldsymbol{m} \mathscr{C}(f) \rangle$ as a function with θ degrees of freedom. This can be done if there exists a function such that $f(t, \mathbf{x}, \boldsymbol{\xi}) = F(\langle \mathbf{m} f \rangle, \boldsymbol{\xi})$. With this function, the fluxes and collisions terms can also be expressed in terms of the densities. Hence, the number of moments are equal to the degrees of freedom (unknowns). The closed system has the form,

$$\partial_t \langle \mathbf{m} F \rangle + \partial_{x_j} \langle \xi_j \mathbf{m} F \rangle = \langle \mathbf{m} \mathscr{C}(F) \rangle \tag{3.13}$$

Note that f is an element of an infinite dimensional vector space and cannot be expressed by a finite number of components. Therefore, any closure will require the approximation of f. The goal is to find an approximation that, in addition to providing well-posedness of (3.13), maintains the key properties of (3.1). That is, every closure approximation should yield a system such that [19],

1. Each member of the hierarchy is hyperbolic and should satisfy some local dissipation relation.

2. Collisional terms are approximated such that each member of the hierarchy beyond the second recover the correct Navier-Stokes behavior

To attain these properties, some requirements needs to be imposed on the space $\mathbb{M}$,

I) $\mathbb{E} \equiv \text{span}\{1, \boldsymbol{\xi}, |\boldsymbol{\xi}|^2\} \subset \mathbb{M}$:
The span denotes all the linear combination of their components. The space $\mathbb{M}$ contains the collection of collision invariants $\mathbb{E}$. Any moment closure will include the conservation of mass, momentum and energy which is need if any fluid dynamical approximation is to be recovered.

II) $\mathbb{M}$ is invariant under the actions of $\mathscr{T}_u$ and $\mathscr{T}_o$:
The space should be Galilean invariant, which means that $\mathbb{M}$ does no change when $\boldsymbol{\xi} \to \boldsymbol{\xi} - \mathbf{u}$ and $\boldsymbol{\xi} \to O^T \boldsymbol{\xi}$ for all $\boldsymbol{\xi} \in \mathbb{R}^D$ and orthogonal matrices $O \in \mathbb{R}^{D \times D}$

III) The set $\mathbb{M}_c \equiv \{m \in \mathbb{M} : \langle F(t, \boldsymbol{x}, m(\boldsymbol{\xi})) \rangle < \infty\}$ has a nonempty interior in $\mathbb{M}$:
This requirement implies that $\mathbb{M}$ contains suitable functions to ensure integrability. Thus the subspace $\mathbb{M}_c$ of $\mathbb{M}$ consists of polynomials $m(\boldsymbol{\xi})$ for which $F(t, \boldsymbol{x}, m(\boldsymbol{\xi})) \to 0$ as $|\boldsymbol{\xi}| \to \infty$.

Subspaces that satisfy the aformentioned properties are called *admissible* and all the other space *inadmissible*. Examples of admissible subspaces with maximal degree two and four are,

$$\begin{aligned}
\text{Maximal degree} = 2: \quad & \mathbb{M} = \text{span}\{1, \boldsymbol{\xi}, |\boldsymbol{\xi}|^2\} \equiv \mathbb{E} \\
& \mathbb{M} = \text{span}\{1, \boldsymbol{\xi}, \boldsymbol{\xi} \otimes \boldsymbol{\xi}\} \\
\text{Maximal degree} = 4: \quad & \mathbb{M} = \text{span}\{1, \boldsymbol{\xi}, \boldsymbol{\xi} \otimes \boldsymbol{\xi}, |\boldsymbol{\xi}|^2 \boldsymbol{\xi}, |\boldsymbol{\xi}|^4\} \\
& \mathbb{M} = \text{span}\{1, \boldsymbol{\xi}, \boldsymbol{\xi} \otimes \boldsymbol{\xi}, \boldsymbol{\xi} \otimes \boldsymbol{\xi} \otimes \boldsymbol{\xi}, |\boldsymbol{\xi}|^4\}
\end{aligned}$$

In two spatial dimensions (considered in this thesis), the admissible subspaces have dimensions 4, 6, 9 and 11 respectively.

3.3 Closure procedure

In the previous section the function $F(\langle \mathbf{m}f\rangle, \boldsymbol{\xi})$ was introduced in order to give the closed system of moment equations (3.13). Now this function needs to be made known for which an entropy minimization principle will be used. Entropy can be understood to represent the number of possible arrangements of gaseous particles in phase space corresponding to a given velocity distribution function. If all the particle arrangements occur with the same frequency, the velocity distribution functions with the lowest entropy will be the most likely. Thus if the distribution function of a gas is needed, the best choice is the one which has the minimum entropy and satisfy the known properties of the gas. It should be mentioned that some authors prefer to talk about maximum entropy which is equivalent to the minimum entropy but multiplied with a minus sign [21].
Following the results of [18, 19], Boltzmann's celebrated H-Theorem will be used to obtain the minimum entropy. The entropy is denoted by $\mathcal{H} = \mathcal{H}(f) := \langle f\ln f - f\rangle$, the flux by $\phi_j = \phi_j(f) := \langle \xi_j f\ln f - \xi_j f\rangle$ and its production term by $\sigma = \sigma(f) := \langle \ln f \mathscr{C}(f)\rangle$. The second directional derivative of $\mathcal{H}(f)$ is,

$$\frac{d^2}{d\epsilon^2}\mathcal{H}(f+\epsilon\psi)\Big|_{\epsilon=0} = \left\langle \frac{\psi^2}{f}\right\rangle > 0 \tag{3.14}$$

for all functions ψ. This implies that $\mathcal{H}(f)$ is a strictly convex functional. Relation (3.5) implies that solutions to the Boltzmann equation formally satisfy the local dissipation law and thus corresponding to,

$$\partial_t \mathcal{H} + \partial_{x_j}\phi_j = \sigma \leq 0 \tag{3.15}$$

The minimum entropy distribution function $F(\langle \mathbf{m}f\rangle, \boldsymbol{\xi})$ is defined as the minimizer for the entropy $\mathcal{H}(f)$ subject to the constraint that it yields a given finite set of velocity moments. The entropy minimization problem is therefore,

$$\underset{g\in\mathcal{F}}{\operatorname{argmin}}\{\mathcal{H}(g) : \langle \boldsymbol{m}g\rangle = \boldsymbol{\rho}\} \tag{3.16}$$

with $\boldsymbol{\rho} := \langle \boldsymbol{m}f\rangle$ the velocity moments of f corresponding to the macroscopic properties. If the minimum entropy distribution F exist then it satisfies (3.15) [18]. The closure obtained by entropy minimization is called a *entropy-based closure*. The minimization problem can be solved by using the technique of Lagrange multipliers. Introducing a vector of Langrange multipliers $\boldsymbol{\lambda}$, the problem becomes a search of finding the stationairy points of the function $\Lambda(g, \boldsymbol{\lambda})$, having the form,

$$\Lambda(g, \boldsymbol{\lambda}) = \mathcal{H}(g) + \boldsymbol{\lambda}\cdot(\boldsymbol{\rho} - \langle \boldsymbol{m}g\rangle) \tag{3.17}$$

At a critical point, the directional derivative is zero, thus

$$\frac{d\Lambda}{dg} = \ln g - \boldsymbol{\lambda}\cdot\boldsymbol{m} = 0 \tag{3.18}$$

This implies that the minimizer F is given by,

$$F(\boldsymbol{\rho}, \boldsymbol{\xi}) = g = \exp(\boldsymbol{\lambda}(\boldsymbol{\rho})\cdot\boldsymbol{m}(\boldsymbol{\xi})) \tag{3.19}$$

Recalling requirement (III) from the previous section, $\exp(\boldsymbol{\lambda}\cdot\boldsymbol{m})$ is integrable if $\boldsymbol{\lambda}\cdot\boldsymbol{m}$ lies in $\mathbb{M}_c$. The closed moment system can be written as,

$$\partial_t\big\langle \mathbf{m}(\boldsymbol{\xi})F(\boldsymbol{\rho},\boldsymbol{\xi})\big\rangle + \partial_{x_j}\big\langle \xi_j\mathbf{m}(\boldsymbol{\xi})F(\boldsymbol{\rho},\boldsymbol{\xi})\big\rangle = \big\langle \mathbf{m}(\boldsymbol{\xi})\mathscr{C}(F(\boldsymbol{\rho},\boldsymbol{\xi}))\big\rangle \tag{3.20}$$

with $F \in \mathcal{F}_{\boldsymbol{m}} \subset \mathcal{F}$ given by,

$$\mathcal{F}_{\boldsymbol{m}} := \{g \in \mathcal{F} : \langle \boldsymbol{m}g\rangle = \boldsymbol{\rho}\} \tag{3.21}$$

The problem with the entropy-based closure given above is that for useful choices of the basis vector $\boldsymbol{m}(\boldsymbol{\xi})$ such that $\{m_i\}_{i=1}^{\theta}$ span some admissible space, the set defined by densities corresponding to physically realizable values of $\boldsymbol{\rho}$ for which the minimizer (3.16) does not exist is non-empty [19]. The set of densities for which this holds are called *degenerate* densities. Hence, this implies that for those densities the exponential closure can not be obtained as the solution of the entropy minimization problem (3.16).

An important aspect in finding a closed form of the moment system is that any resulting moment closure system should be well-posed and that it retains the fundamental properties of the Boltzmann equation. This implies that,

1. The moment closure system (3.20) is a symmetric hyperbolic system
2. Solutions to the moment closure system (3.20) satisfy the dissipation relation (3.15)
3. Equality in the dissipation relation (3.15) is attained if and only if F is a Maxwellian density given by (3.6)
4. The moment closure system (3.20) retains conservation of mass, momentum and energy as well as Galilean invariance

In circumstances that the entropy minimization problem (3.16) admits a solution, the closed moment system (3.20) satisfy all these requirements for which the proofs can be found [18] and [19, chapter 2].

As mentioned, the assumption that there exist a minimum entropy distribution for the minimization problem (3.16) does not always holds. There are realizable values $\boldsymbol{\rho}$ for which no Langrange multipliers $\boldsymbol{\lambda}$ can be found such that $\boldsymbol{\rho} = \langle \mathbf{m}\exp(\boldsymbol{\lambda}\cdot\boldsymbol{m})\rangle$. To be more precise, for any moment system that include super-quadratic polynomial moments, the set containing all degenerate densities is non-empty. However, moment systems with super-quadratic polynomials moments are needed in order to obtain the heat flux or the stress tensor.

To circumvent the problem with degenerate densities, one can consider two possibilities. The first one is to ensures that the values corresponding to degenerate densities will never be attained in the moment system generated by the entropy closure. The second one is a relaxation of the entropy minimization problem (3.16). The details for the second case can also be found in [19, chapter 2].

Another problem associated with minimal-entropy closure, pertains to computability of moments. Consider a moment system containing super-quadratic polynomials moments and

for which there exists a solution to the minimization problem (3.16) given some realizable values $\boldsymbol{\rho}$. Suppose that this minimizer is given by $F = \exp(\lambda_0 + \lambda_1\xi + \lambda_2\xi^2 + \lambda_3\xi^3 + \lambda_4\xi^4)$. To obtain the macroscopic properties, one needs to calculate its moments which includes integration over the velocity domain. However, this is a notoriously difficult problem since the distribution function F contains a super-quadratic velocity polynomial. This problem has been investigated in [19] in which the author proposed a new class of moment closure approximation which makes the moment system more tractable. An entropic projection $\mathcal{E}$ of the same exponential form can be factorized such that the entropy minimization distribution can be written as,

$$F = \mathcal{E}(\boldsymbol{\lambda}_0)\exp((\boldsymbol{\lambda} - \boldsymbol{\lambda}_0)\cdot\boldsymbol{m}) \tag{3.22}$$

with $\mathcal{E}$ corresponding to a global or local equilibrium distribution for which $\boldsymbol{\lambda}_0$ is known. Using the limit definition of the exponential function gives,

$$F = \mathcal{E}(\boldsymbol{\lambda}_0)\lim_{n\to\infty}\Big(1 + \frac{(\boldsymbol{\lambda} - \boldsymbol{\lambda}_0)\cdot\boldsymbol{m}}{n}\Big)^n \tag{3.23}$$

Truncation of the limit at some N will give the approximated distribution $\widetilde{F}$,

$$\widetilde{F} = \mathcal{E}(\boldsymbol{\lambda}_0)\Big(1 + \frac{\boldsymbol{\lambda}_1\cdot\boldsymbol{m}}{N}\Big)^N \tag{3.24}$$

with $\boldsymbol{\lambda}_1$ the unkown Langrange multipliers. Applying this approximation to the closed moment system (3.20) yields an approximation of the closed moment system,

$$\begin{aligned}\partial_t\Big\langle \mathbf{m}(\boldsymbol{\xi})\mathcal{E}(\boldsymbol{\lambda}_0)\Big(1 + \frac{\boldsymbol{\lambda}_1\cdot\boldsymbol{m}}{N}\Big)^N\Big\rangle + \partial_{x_j}\Big\langle \xi_j\mathbf{m}(\boldsymbol{\xi})\mathcal{E}(\boldsymbol{\lambda}_0)\Big(1 + \frac{\boldsymbol{\lambda}_1\cdot\boldsymbol{m}}{N}\Big)^N\Big\rangle \\ = \Big\langle \mathbf{m}(\boldsymbol{\xi})\mathscr{C}(\mathcal{E}(\boldsymbol{\lambda}_0)\Big(1 + \frac{\boldsymbol{\lambda}_1\cdot\boldsymbol{m}}{N}\Big)^N\Big\rangle\end{aligned} \tag{3.25}$$

The author has shown that the above system still satisfies the properties of the Boltzmann equation namely, dissipation of a modified entropy and hyperbolicity. These proofs will not be shown here but can be found in [19, chapter 3].

Within this work, the equilibrium distribution $\mathcal{E}$ will correspond to a Maxwellian distribution $\mathcal{M}$ such that the entropy minimization distribution is given by,

$$\widetilde{F} = \mathcal{M}(\boldsymbol{\lambda}_0)\Big(1 + \frac{\boldsymbol{\lambda}_1\cdot\boldsymbol{m}}{N}\Big)^N \tag{3.26}$$

Chapter 4

Collision integral

One of the main difficulties to deal with the Boltzmann equation is the expression of the collision term, which is given by [8],

$$\mathscr{C}(f) = \int_{\mathbb{R}^3} \int_{\mathcal{B}^-} \{f' f'_* - f f_*\} \mathcal{B}(\Theta, V) d\boldsymbol{\xi}_* d\Theta d\epsilon \tag{4.1}$$

Its dependence on two different density functions f and f' and the quadratic nonlinearity of the density functions makes it a complicated structure. Therefore, the evaluation of this collision term in order to find solutions of the Boltzmann equation, is quite a challeging proposition. As a consequence, different kind of models have been developed over the years which replace the collision term by a collision model. Those models seek to maintain the fundamental properties but try to make direct evaluation simpler.
The most widely studied and well-known collision model is the BGK model, named after those who proposed it Bhatnagar, Gross and Krook [25]. The BGK model is given by,

$$\widetilde{\mathscr{C}}(f) = \nu(\mathcal{M} - f) \tag{4.2}$$

with ν a positive collision frequency which is independent of $\boldsymbol{\xi}$ but depends on the density ρ and the temperature T. $\mathcal{M}$ is the Maxwellian distribution function (3.6) constructed from the first three moments of f. This implies that the density ρ, velocity $\boldsymbol{u}$ and temperature T of $\mathcal{M}$ and f are the same.
Note that the nonlinearity of the BGK model is worse than the nonlinearity of the collision integral $\mathscr{C}(f)$. $\mathscr{C}(f)$ is only quadratic in f whereas in the BGK model, f appears in the numerator and in the denominator of the Maxwellian $\mathcal{M}$. Although this disadvantage, the BGK model is still considerably more tractable than the original collision integral and the evaluation will be no harder than the fluxes. One of the major disadvantage is that the BGK model predicts a Prandtl number ($Pr = c_p\mu/\kappa$ with c_p the specific heat at constant temperature) of one rather than a value close to 2/3 appropriated for monatonic gases [18]. This implies that the model can not match the viscosity μ and the thermal conductivity κ of a real gas the same time.

Other models have been developed to recover the correct Prandtl number. One of those models is describe by Holway [8], which proposed the so-called ellipsoidal statistical BGK model (ES-BGK). In this model, the Maxwellian distribution $\mathcal{M}$ in (4.2) is replaced by an

anisotropic Gaussian distribution $\mathcal{G}$ given by,

$$\mathcal{G}(\rho, \boldsymbol{u}, \boldsymbol{\mathcal{T}}) = \frac{\rho}{\sqrt{\det(2\pi\boldsymbol{\mathcal{T}})}} \exp\left(\frac{-(\boldsymbol{\xi}-\boldsymbol{u})\cdot\boldsymbol{\mathcal{T}}^{-1}(\boldsymbol{\xi}-\boldsymbol{u})}{2}\right)$$

with $\boldsymbol{\mathcal{T}}$ given by,

$$\boldsymbol{\mathcal{T}} = \frac{RT}{MPr}\boldsymbol{I} - \frac{(1-Pr)\boldsymbol{p}}{\rho Pr}$$

Note that if $Pr = 1$, then one will recover the BGK model. Two other models which recover the proper Prandtl number are given by Lebowitz, Frisch and Helfand called the integro-differential model and by Struchtrup called the BGK model with velocity-dependent collision frequency [8,26]. Numerical comparison between the BGK model, ES-BGK model and some other models can be found in [1,24].
A new approach is given by Levermore which introduces in [18] a generalization of the BGK model. This model adds different relaxation terms towards "generalized" Maxwellians corresponding to different collision frequencies ν_i.
Although all these models improve the approximation of the Prandtl number w.r.t. the BGK model, the work in this thesis does not require accurate estimation of the Prandtl number. Therefore, the focus will be on the original BGK model.

4.1 Properties of the BGK model

The collision operator $\mathscr{C}(f)$ satisfy three fundamental properties which were treated in section 3.1.1. Any approximation of the collision operator needs to satisfy these properties and thus it remains to check whether this is the case for the BGK operator (4.2).

1. ***Conservation of Mass, Momentum and Energy***
   It can be observed that the BGK operator $\widetilde{\mathscr{C}}(f)$ has $\gamma \in \{1, \boldsymbol{\xi}, |\boldsymbol{\xi}|^2\}$ as locally conserved quantities and thus satisfying,

   $$\left\langle \gamma \mathscr{C}(f) \right\rangle = 0 \qquad \forall f \in \mathscr{D}(\mathscr{C})$$

   Using the result below, equation (4.3), the only way that the integral can vanish is when $f = \mathcal{M}$ since $\nu > 0$. Thus the only locally conserved quantities are those in $\mathbb{E} = \{1, \boldsymbol{\xi}, |\boldsymbol{\xi}|^2\}$, thereby showing the equivalence between statements (3.3) and (3.4).

2. ***Dissipation of entropy: H-theorem***
   It needs to be verified that if $\widetilde{\mathscr{C}}(f)$ multiplied by $\ln f$ and integrate over the whole velocity domain, the results is smaller or equal to zero for all $f \in \mathscr{D}(\mathscr{C})$. Let $\boldsymbol{g} \in \mathbb{E} \equiv \text{span}\{1, \boldsymbol{\xi}, |\boldsymbol{\xi}|^2\}$, since the first three moments of $\mathcal{M}$ and f are the same it follows that, $\left\langle (\mathcal{M}-f)\boldsymbol{g} \right\rangle = 0$. Note that, $\ln\mathcal{M} \in \mathbb{E}$ and thus $\left\langle (\mathcal{M}-f)\ln\mathcal{M} \right\rangle = 0$. Using this relation,

   $$\begin{aligned} \left\langle \widetilde{\mathscr{C}}(f)\ln f \right\rangle &= \left\langle \nu(\mathcal{M}-f)\ln f \right\rangle \\ &= \left\langle \nu(\mathcal{M}-f)\ln\frac{f}{\mathcal{M}} \right\rangle \leq 0 \end{aligned} \tag{4.3}$$

   where the inequality is obtained by using $\forall x, y \in \mathbb{R}$, $(y-x)\ln\frac{x}{y} \leq 0$.

3. ***Galilean invariance***
   The BGK operator $\widetilde{\mathscr{C}}(f)$ commute with the translational and rotational tranformation since $\mathbb{E}$ is an admissible space, implying that $\mathbb{E}$ is Galilean invariant.

The collision frequency ν in equation (4.2) is sometimes written as $1/\tau$ with τ the relaxation time. Following Levermore [18], the frequency is given by $\nu = \rho\Theta/\mu(\rho, \Theta)$, with μ the dynamic viscosity. Using this frequency, the correct Navier-Stokes equations can be recovered as a first-order correction to the Euler equations by using a Chapman-Enskog expansion. Thus if the Navier-Stokes viscosity is known, the collision term can be computed very easily. But the viscosity can only be otained by solving the Navier-Stokes equations which makes solving the Boltzmann equation needless. Moreover, for simulations within the rarefied regime, the viscosity is not known since the Navier-Stokes is not applicable anymore.

The most usefull solution would be a relation between the Knudsen number Kn and the frequency ν. This result is included in Bird [3] and Chen [11]. Herein, the viscosity obtained from the transport theory of Chapman-Enskog, is given for the hard sphere model. This model assumes that the particles are spherical, moving along straight lines and collide elastically, like billiard balls. The viscosity is given by,

$$\mu = \frac{5}{16}\sqrt{\pi m k T}\frac{1}{\pi d^2}$$

with m the molecular mass, k the Boltzmann constant and T the temperature. To eliminated the cross section πd^2, the following definition of the mean free path λ will be used [31],

$$\lambda = \frac{1}{\sqrt{2}\pi d^2 n} \tag{4.4}$$

with n=N/V denotes the number of molecules per unit volume and "d" the diameter of the molecule. Using this relation and $kT = \Theta m$ we obtain,

$$\lambda = \frac{16\mu}{5}\sqrt{\frac{1}{2\pi\rho^2\Theta}}$$

where $\rho = nm$ is the gas density. Replacing the viscosity by $\mu = \rho\Theta/\nu = \rho\Theta\tau$ to obtain,

$$\lambda = \frac{16\tau}{5}\sqrt{\frac{\rho^2\Theta^2}{2\pi\rho^2\Theta}} = \frac{16\tau}{5}\sqrt{\frac{\Theta}{2\pi}} = \frac{16\tau}{5}\sqrt{\frac{P}{2\pi\rho}}$$

with $P = \rho\Theta$. The relaxation time can now be related to the Knudsen number,

$$\tau = \frac{5KnL}{16}\sqrt{\frac{2\pi\rho}{P}} \tag{4.5}$$

Here, L is the typical length scale which will be equal to one for all the simulations. The same result is obtained in the paper of McDonald [20]. The relaxation time for a similation is fixed in time and the values for the pressure P and density ρ are determined locally during the computation; See chapter 2.

Chapter 5

Numerical scheme

In this section, we present a numerical scheme for finding solutions of the closed moment system (3.25). Since this thesis is devoted to obtaining solutions for higher spatial dimension, we consider the spatial domain $\Omega \subset \mathbb{R}^d$ with $d = 1, 2$. Although the one-dimensional case has been investigated in different papers, see for example [23], [22] and [5], the moment closure approach in this work is different and is therefore included as well.

5.1 Discontinuous Galerkin

The system of partial differential equations we are dealing with belongs to the class of hyperbolic equations. In general, the solutions to these class of equations can be discontinuous. The Discontinuous Galerkin method (DG) will therefore be the most suitable method. Like in the classical Finite Element Methods (FEM), the unknowns are represented by piecewise polynomial functions. Whereas in the FEM, the polynomials are continuous across the element interface, for the DG method the polynomials are discontinous at the interfaces. Therefore, the solution itself is discontinuous (double-valued) at the element boundaries as well as the fluxes. Since the flux is not allowed to be double-valued, in order to uniquely define the boundary integral of the flux, a numerical flux will be defined.

Let Ω be the spatial domain subdivided into finite-size elements κ_i and denote by $\mathcal{T} = \{\kappa_1, \kappa_2, ...\}$ the element set. Assume that the elements κ_i are stationary, and non-overlapping [2], [19]:

- $\overline{\Omega} \equiv \bigcup_{\kappa_i \in \tau} \kappa_i$
- $\kappa_i \cap \kappa_j = \emptyset, \quad i \neq j$

The discretized domain is denoted by Ω^h. For the geometries considered in this thesis, the domain Ω is identical to Ω^h. However, for more complex geometries the discretized domain Ω^h will be an approximation for the physical domain Ω. Let $\mathcal{P}^k(Q)$ denote the set of polynomials of degree at most $k \geq 0$ in a domain $Q \subset \mathbb{R}^d$. Using the DG method, the following finite element space will be used,

$$\mathcal{V}_h^k = \{\mathbf{w} : \forall \kappa \in \tau, \mathbf{w}|_k \in (\mathcal{P}^k)^\theta\} \tag{5.1}$$

with θ the dimension of the vector $\mathbf{m}(\mathbf{v})$. Note that $\mathcal{V}_h^k$ contains piecewise discontinuous polynomials.

5.1.1 Strong formulation

First introduce the following shorthand notations,

$$\boldsymbol{U}(\boldsymbol{\lambda}) = \langle \mathbf{m}\widetilde{F} \rangle \qquad \boldsymbol{\mathcal{J}}_j(\boldsymbol{U}(\boldsymbol{\lambda})) = \langle \xi_j \mathbf{m}\widetilde{F} \rangle \qquad \boldsymbol{\mathcal{Q}}(\boldsymbol{U}(\boldsymbol{\lambda})) = \langle \mathbf{m}\mathscr{C}(\widetilde{F}) \rangle$$

with $\widetilde{F}$ given by (3.24). The closed moment system (3.25) can be rewritten as,

$$\partial_t \boldsymbol{U} + \partial_{x_j} \boldsymbol{\mathcal{J}}_j(\boldsymbol{U}) = \boldsymbol{\mathcal{Q}}(\boldsymbol{U}) \tag{5.2}$$

Complementing it with an initial condition to set up Cauchy's initial value problem,

$$\mathcal{P} \begin{cases} \partial_t \boldsymbol{U} + \partial_{x_j} \boldsymbol{\mathcal{J}}_j(\boldsymbol{U}) = \boldsymbol{\mathcal{Q}}(\boldsymbol{U}), & \Omega \times [t^0, t^N] \\ \boldsymbol{U}(\boldsymbol{\lambda}(\boldsymbol{x}, t^0)) = \boldsymbol{U}_0(\boldsymbol{x}) \end{cases} \tag{5.3}$$

Supplemented with the convex entropy extension of the form given in (3.15). As discussed in the previous chapter, the collision operator, $\mathscr{C}(F)$ will be replaced by the BGK operator $\widetilde{\mathscr{C}}(F)$ such that the collision term $\boldsymbol{\mathcal{Q}}(\boldsymbol{U})$ is given by,

$$\boldsymbol{\mathcal{Q}} = \langle \mathbf{m}\widetilde{\mathscr{C}}(\widetilde{F}) \rangle = -\frac{1}{\tau}\big(\langle \mathbf{m}\widetilde{F} \rangle - \langle \mathbf{m}\mathcal{M} \rangle\big) \tag{5.4}$$

with τ the relaxation time given in (4.5) and $\mathcal{M}$ a Maxwellian distribution.

5.1.2 Weak formulation

To obtain the weak formulation for the DG finite-element method from the strong form (5.2), the following consecutive steps needs to be performed,

Step 1: *multiplying with a test function $\boldsymbol{\phi}(\mathbf{x}) \in \mathcal{V}_h^k$ and integrate over Ω*

$$\int_\Omega \boldsymbol{\phi} \cdot \partial_t \boldsymbol{U}(\boldsymbol{\lambda})\, dx + \int_\Omega \boldsymbol{\phi} \cdot \partial_{x_j} \boldsymbol{\mathcal{J}}_j(\boldsymbol{\lambda})\, dx = \int_\Omega \boldsymbol{\phi} \cdot \boldsymbol{\mathcal{Q}}(\boldsymbol{\lambda})\, dx \tag{5.5}$$

Step 2: *replace integral over space with summation over the elements κ*

$$\sum_\kappa \int_\kappa \boldsymbol{\phi} \cdot \partial_t \boldsymbol{U}(\boldsymbol{\lambda})\, dx + \sum_\kappa \int_\kappa \boldsymbol{\phi} \cdot \partial_{x_j} \boldsymbol{\mathcal{J}}_j(\boldsymbol{\lambda})\, dx = \sum_\kappa \int_\kappa \boldsymbol{\phi} \cdot \boldsymbol{\mathcal{Q}}(\boldsymbol{\lambda})\, dx \tag{5.6}$$

Step 3: *applying the product rule*

$$\begin{aligned} \sum_\kappa \int_\kappa \boldsymbol{\phi} \cdot \partial_t \boldsymbol{U}(\boldsymbol{\lambda})\, dx \;\; &+ \;\; \sum_\kappa \int_\kappa \partial_{x_j} \Big(\boldsymbol{\phi} \cdot \boldsymbol{\mathcal{J}}_j(\boldsymbol{\lambda}) \Big)\, dx - \sum_\kappa \int_\kappa \boldsymbol{\mathcal{J}}_j(\boldsymbol{\lambda}) \cdot \partial_{x_j} \boldsymbol{\phi}\, dx \\ &= \;\; \sum_\kappa \int_\kappa \boldsymbol{\phi} \cdot \boldsymbol{\mathcal{Q}}(\boldsymbol{\lambda})\, dx \end{aligned} \tag{5.7}$$

Step 4: *applying the Gauss divergence theorem and replace the flux $\boldsymbol{\mathcal{J}}_j$ within the integral over the element boundary $\partial\kappa$ with the numerical flux $\widetilde{\boldsymbol{\mathcal{J}}}_j$*

$$\sum_\kappa \int_\kappa \boldsymbol{\phi} \cdot \partial_t \boldsymbol{U}(\boldsymbol{\lambda})\, dx \;+\; \sum_\kappa \int_{\partial\kappa} \boldsymbol{\phi} \cdot \widetilde{\boldsymbol{\mathcal{J}}}_j(\boldsymbol{\lambda}(x_-), \boldsymbol{\lambda}(x_+); \boldsymbol{n})\, ds - \sum_\kappa \int_\kappa \boldsymbol{\mathcal{J}}_j(\boldsymbol{\lambda}) \cdot \partial_{x_j} \boldsymbol{\phi}\, dx - \sum_\kappa \int_\kappa \boldsymbol{\phi} \cdot \boldsymbol{\mathcal{Q}}(\boldsymbol{\lambda})\, dx = 0 \tag{5.8}$$

with $\partial\kappa$ the boundaries of element κ. Here, $x_{-/+}$ denotes the left and right interface states. Denote the left hand side of (5.8) by $B(\boldsymbol{\lambda}, \boldsymbol{\phi})$ then the problem statements is as follows,

$$\text{Find } \boldsymbol{\lambda}(x,t) \in \mathcal{V}_h^k \text{ such that } B(\boldsymbol{\lambda}, \boldsymbol{\phi}) = 0, \qquad \forall \boldsymbol{\phi} \in \mathcal{V}_h^k \tag{5.9}$$

Note that the summation of the boundary integral ∂_κ can also be rewritten as,

$$\sum_\kappa \int_{\partial\kappa} \boldsymbol{\phi} \cdot \widetilde{\boldsymbol{\mathcal{J}}}_j(\boldsymbol{\lambda}(x_-), \boldsymbol{\lambda}(x_+); \boldsymbol{n})\, ds = \sum_i \int_{\Sigma_i} \Big(\boldsymbol{\phi}_- \cdot \widetilde{\boldsymbol{\mathcal{J}}}_j(\boldsymbol{\lambda}_-, \boldsymbol{\lambda}_+; \boldsymbol{n}_-) + \boldsymbol{\phi}_+ \cdot \widetilde{\boldsymbol{\mathcal{J}}}_j(\boldsymbol{\lambda}_-, \boldsymbol{\lambda}_+; \boldsymbol{n}_+) \Big)\, d\sigma + \sum_b \int_{\Gamma_b} \boldsymbol{\phi} \cdot \boldsymbol{\mathcal{J}}_j(\boldsymbol{\lambda}^*)\, d\sigma \tag{5.10}$$

with $\boldsymbol{\lambda}_{-/+} = \boldsymbol{\lambda}(x_{-/+})$, $\boldsymbol{n}_{-/+}$ the unit normal vector pointing to the exterior of element $\kappa_{-/+}$. The summation over Σ_i denotes the internal element boundaries and Γ_b the boundaries of the computational domain. $\boldsymbol{\lambda}^*$ is used to weakly prescibe the boundary conditions. By considering that $\boldsymbol{n}_- + \boldsymbol{n}_+ = \boldsymbol{0}$ and using the conservation property of the numerical flux, see section 5.3, equation (5.10) can be rewritten as,

$$\sum_\kappa \int_{\partial\kappa} \boldsymbol{\phi} \cdot \widetilde{\boldsymbol{\mathcal{J}}}_j(\boldsymbol{\lambda}(x_-), \boldsymbol{\lambda}(x_+); \boldsymbol{n})\, ds = \sum_i \int_{\Sigma_i} \big(\boldsymbol{\phi}_- - \boldsymbol{\phi}_+ \big) \cdot \widetilde{\boldsymbol{\mathcal{J}}}_j(\boldsymbol{\lambda}_-, \boldsymbol{\lambda}_+; \boldsymbol{n}_-)\, d\sigma + \sum_b \int_{\Gamma_b} \boldsymbol{\phi} \cdot \boldsymbol{\mathcal{J}}_j(\boldsymbol{\lambda}^*)\, d\sigma \tag{5.11}$$

5.2 Time derivative

For the time derivative $\partial_t \boldsymbol{U}(\boldsymbol{\lambda})$ a forward difference approximation will be used. The forward difference approximation, also called the explicit (or forward) Euler method, is used to approximate the first derivative to either time t or spatial variable x. Let the step size in time be Δt, then the one-step scheme for the ODE $du/dt = f(u,t)$ is,

$$\frac{1}{\Delta t}\big(u^{n+1} - u^n\big) = f(u^n, t^n)$$

with u^n the approximation of the solution u at time t^n. The solution at the new time instant u^{n+1} is defined by the solution at the current time u^n. Using this forward difference approximation, the weak formulation (5.8) can be written as,

$$\int_\Omega \boldsymbol{\phi} \cdot \frac{\boldsymbol{U}(\boldsymbol{\lambda}^{n+1}) - \boldsymbol{U}(\boldsymbol{\lambda}^n)}{\Delta t}\, dx \;+\; \sum_\kappa \int_{\partial\kappa} \boldsymbol{\phi} \cdot \widetilde{\boldsymbol{\mathcal{J}}}_j(\boldsymbol{\lambda}^n(x_-), \boldsymbol{\lambda}^n(x_+); \boldsymbol{n})\, ds - \sum_\kappa \int_\kappa \boldsymbol{\mathcal{J}}_j(\boldsymbol{\lambda}^n) \cdot \partial_{x_j} \boldsymbol{\phi}\, dx = \sum_\kappa \int_\kappa \boldsymbol{\phi} \cdot \boldsymbol{\mathcal{Q}}(\boldsymbol{\lambda}^n)\, dx \tag{5.12}$$

5.3 Numerical flux

The DG method requires no continuity across inter-element boundaries. Thus, let $\partial\kappa = \kappa_j \cap \kappa_i$ with $i \neq j$ be an inter-element boundary then the solution from the left element $\boldsymbol{U}_j$ and right element $\boldsymbol{U}_i$ at the boundary are not the same. The same is true for the fluxes from both elements $\boldsymbol{\mathcal{J}}_j$ and $\boldsymbol{\mathcal{J}}_i$. So the discontinuities at the inter-element boundaries and the boundaries of the computational domain can be conceived as a local Riemann problem. The solution of the local Riemann problem is the best option to determine the numerical fluxes, but can be complicated or numerical expensive. Moreover, there is no need to get the exact solution since the discretization of the domain or other approximations will give to numerical errors. An approximation of the exact solution of the Riemann problem will be almost as good as the exact solution.
Several approximate Riemann solvers have been developed during the last decades, e.g. Rosanov flux (also called Local Lax Friendrichs flux), Roe flux, Harten-Lax-van-Leer and Osher-Solomon, see [30]. The selected numerical flux should satisfy certain conditions: **(1)** satisfy the correct jump condition for the existing shocks, **(2)** satisfy an entropy condition in order to find only physically correct shocks and **(3)** be stable [16]. A numerical flux which satisfy all these conditions is the Osher-Solomon flux. An additional attractive feature is that this flux is very robust.

To uniquely defined the integration over the inter-element boundary and to prescibe the boundary date in a weak sense, a numerical flux needs to be introduced. This is a vector-valued function $\widetilde{\boldsymbol{\mathcal{J}}}(\boldsymbol{\lambda}(x_-), \boldsymbol{\lambda}(x_+); \mathbf{n}) : \mathbb{R}^\theta \times \mathbb{R}^\theta \times \mathbb{R}^D \to \mathbb{R}^\theta$ which is single-valued on the element boundaries. Furthermore, it needs to satisfy the following properties [19],

- *Consistency:* consistency is obtained if the numerical flux reduces to the physical flux if identical state arguments are used for the numerical flux

$$\widetilde{\boldsymbol{\mathcal{J}}}(\boldsymbol{\lambda}(x), \boldsymbol{\lambda}(x); \mathbf{n}) = \boldsymbol{\mathcal{J}}(\boldsymbol{\lambda}) \cdot \mathbf{n}$$

- *Discrete cell conservation:* This property ensures that the fluxes from adjacent cells sharing a mutual interface cancel when summed. This can be written as,

$$\widetilde{\boldsymbol{\mathcal{J}}}(\boldsymbol{\lambda}(x_-), \boldsymbol{\lambda}(x_+); \mathbf{n}) = -\widetilde{\boldsymbol{\mathcal{J}}}(\boldsymbol{\lambda}(x_-), \boldsymbol{\lambda}(x_+); -\mathbf{n})$$

Since the Osher-Solomon flux possess nice properties, it has been used as the numerical flux within this thesis. First let's introduce appropriate notation. A complete review can be found in [13]. The Jacobian matrix of the flux vector $\boldsymbol{\mathcal{J}}$ is given by,

$$\mathbf{A}(\mathbf{U}) = \frac{\partial \boldsymbol{\mathcal{J}}(\boldsymbol{U})}{\partial \mathbf{U}}$$

which can be diagonalized because of the hyperbolicity of the moment system,

$$\mathbf{A}(\mathbf{U}) = \mathbf{R}(\mathbf{U})\boldsymbol{\Lambda}(\mathbf{U})\mathbf{R}^{-1}(\mathbf{U})$$

with $\mathbf{R}(\mathbf{U})$ the matrix containing the right eigenvectors of $\mathbf{A}(\mathbf{U})$, $\mathbf{R}^{-1}(\mathbf{U})$ its inverse and $\boldsymbol{\Lambda}(\mathbf{U})$ a diagonal matrix whose diagonal entries are the real eigenvalues λ_i. Also introduce

the following notations,

$$\begin{aligned} \mathbf{A}^{+}(\mathbf{U}) &= \mathbf{R}(\mathbf{U})\mathbf{\Lambda}^{+}(\mathbf{U})\mathbf{R}^{-\mathbf{1}}(\mathbf{U}) \\ \mathbf{A}^{-}(\mathbf{U}) &= \mathbf{R}(\mathbf{U})\mathbf{\Lambda}^{-}(\mathbf{U})\mathbf{R}^{-\mathbf{1}}(\mathbf{U}) \\ |\mathbf{A}(\mathbf{U})| &= \mathbf{R}(\mathbf{U})|\mathbf{\Lambda}(\mathbf{U})|\mathbf{R}^{-\mathbf{1}}(\mathbf{U}) \end{aligned}$$

here $\mathbf{\Lambda}^{\pm}(\mathbf{U})$ is a diagonal matrix containing only the positive($^{+}$) or negative($^{-}$) eigenvalues and $|\mathbf{\Lambda}(\mathbf{U})|$ contains the absolute value of the eigenvalues $|\lambda_i|$. The classical Osher-Solomon numerical flux is defined as,

$$\widetilde{\boldsymbol{\mathcal{J}}}(\mathbf{U}_j, \mathbf{U}_{j+1}) = \boldsymbol{\mathcal{J}}^{+}(\boldsymbol{U_j}) + \boldsymbol{\mathcal{J}}^{-}(\boldsymbol{U_{j+1}}) \tag{5.13}$$

with corresponding Jacobians

$$\mathbf{A}^{+}(\mathbf{U}) = \frac{\partial \boldsymbol{\mathcal{J}}^{+}(\mathbf{U})}{\partial \mathbf{U}}, \qquad \mathbf{A}^{-}(\mathbf{U}) = \frac{\partial \boldsymbol{\mathcal{J}}^{-}(\mathbf{U})}{\partial \mathbf{U}} \tag{5.14}$$

Functions with satisfy (5.13) and (5.14) are in general difficult or impossible to find. However, combining (5.13) and (5.14), the numerical Osher-Solomon flux can be rewritten as,

$$\widetilde{\boldsymbol{\mathcal{J}}}(\mathbf{U}_j, \mathbf{U}_{j+1}) = \frac{1}{2}\big(\boldsymbol{\mathcal{J}}(\mathbf{U}_j) + \boldsymbol{\mathcal{J}}(\mathbf{U}_{j+1})\big) - \frac{1}{2}\int_{\boldsymbol{U}_j}^{\boldsymbol{U}_{j+1}} \big|\mathbf{A}(\mathbf{U})\big| d\mathbf{U} \tag{5.15}$$

In order to use the above numerical flux, the integral in phase-space needs to be evaluated. Note that the integration depends on the chosen path. To make this integration more tractable and to keep is nice properties, Dumbser and Toro [13] choose to connect the two states by a linear path $\mathbf{\Psi}(s) = \mathbf{U}_j + s\big(\mathbf{U}_{j+1} - \mathbf{U}_j\big)$ with $0 \leq s \leq 1$. This function is Lipschitz continuous and satisfies $\mathbf{\Psi}(0) = \mathbf{U}_j$ and $\mathbf{\Psi}(1) = \mathbf{U}_{j+1}$. With this straight line path $\mathbf{\Psi}(s)$, the numerical flux is defined by,

$$\widetilde{\boldsymbol{\mathcal{J}}}(\mathbf{U}_j, \mathbf{U}_{j+1}) = \frac{1}{2}\big(\boldsymbol{\mathcal{J}}(\mathbf{U}_j) + \boldsymbol{\mathcal{J}}(\mathbf{U}_{j+1})\big) - \frac{1}{2}\Big(\int_0^1 \big|\mathbf{A}(\mathbf{\Psi}(s))\big| ds\Big)(\mathbf{U}_{j+1} - \mathbf{U}_j) \tag{5.16}$$

To avoid analytical integration, the integral will be evaluated numerically with a Gauss-Legendre quadrature rule. Let s_j be the integration points and w_j its weights in the interval $I = [0, 1]$, the generalized numerical Osher-Solomon flux can be expressd as,

$$\widetilde{\boldsymbol{\mathcal{J}}}(\mathbf{U}_j, \mathbf{U}_{j+1}) = \frac{1}{2}\big(\boldsymbol{\mathcal{J}}(\mathbf{U}_j) + \boldsymbol{\mathcal{J}}(\mathbf{U}_{j+1})\big) - \frac{1}{2}\Big(\sum_{j=1}^{G} w_j \big|\mathbf{A}(\mathbf{\Psi}(s_j))\big|\Big)(\mathbf{U}_{j+1} - \mathbf{U}_j) \tag{5.17}$$

with G as the total number of integration points. It can be observed that the complete eigenstructure of the system at the integration points are needed to compute the flux. Although in this thesis it was not difficult to compute these numerically there can be systems for which this is difficult. For those situations, Castro et. al. [6] proposed a way in which the absolute value of the Jacobian matrix is approximated.

5.4 Boundary conditions

For simulation of gas flows in a bounded domain or around bodies, the Boltzmann equation must be accompanied with boundary conditions to obtain accurate solutions. The boundary conditions describe the interaction of the gas with the a surface, in this case a solid wall. However, to write down the correct boundary conditions is a difficult task. It needs the knownledge of the structure of surface layers of the solid walls. If a particle impinges upon a surface, it is absorbed and may form chemical bonds, become ionized or displace surface particles. The smoothness and temperature of the surface also influence the interaction as well as heating the surface. So all those dependencies makes it a physical complex problem for both theoritical and experimental research. Therefore, the gas-surface interaction is an area of research by itself [8, 11].

As mentioned in the previous section, a numerical flux needs to be introduced because of the DG method. The inter-element boundaries containing a flux $\boldsymbol{\mathcal{J}}$ from the left and right element. Something similar happens at the boundaries, but only the outgoing flux $\boldsymbol{\mathcal{J}}$ is given. This is the flux from the element within the domain. The incoming flux needs to be imposed. So defined the outgoing and incoming half fluxes as,

$$\boldsymbol{\mathcal{J}}^{+/-} = \int_{\boldsymbol{\xi}\cdot\mathbf{n}\geq 0/\boldsymbol{\xi}\cdot\mathbf{n}\leq 0} \boldsymbol{m}(\boldsymbol{\xi}) \otimes \boldsymbol{\xi} F d\boldsymbol{\xi}$$

with $\mathbf{n}$ the outward unit normal vector. The incoming flux is defined by specifing the incoming distribution F. In Le Tallec et. al. [28], [29], three different types of incoming distributions are defined, which are simple and usefull for practical applications. All these types will be discussed below. Furthermore, let $f^+ = f(\mathbf{x}, \boldsymbol{\xi}, t)_{|\boldsymbol{\xi}\cdot\mathbf{n}\geq 0}$ and $f^- = f(\mathbf{x}, \boldsymbol{\xi}, t)_{|\boldsymbol{\xi}\cdot\mathbf{n}\leq 0}$ the distribution of the incident particles and the reflected particles.

- *Specular reflection*
  This model assumes that the surface is perfectly smooth and that the particles reflect off of the wall are elastic spheres, which implies that the normal to the surface reverses its direction. Thus the angle of the reflected particle is similar to the angle of incidence and the magnitude of the velocity is the same but its direction is reversed. The velocity of the reflected particle is, $\boldsymbol{\xi}' = \mathcal{R}\boldsymbol{\xi} = \boldsymbol{\xi} - 2(\boldsymbol{\xi}\cdot\mathbf{n})\mathbf{n}$, with $\boldsymbol{\xi}$ the velocity of incidence. In terms of the distribution function f, this becomes,

  $$f(\mathbf{x}, \boldsymbol{\xi}', t) = f(\mathbf{x}, \mathcal{R}\boldsymbol{\xi}, t), \qquad \forall \boldsymbol{\xi}' \text{ with } \boldsymbol{\xi}'\cdot\mathbf{n} \leq 0$$

- *Reflection with full accommodation*
  Once the particles are absorbed by the surface, they will be re-emitted with a Maxwellian distribution.

  $$f^-(\xi) = \mathcal{M}[\rho, \mathbf{u}_W, \Theta_W](\boldsymbol{\xi}) = \frac{\rho}{(2\pi\Theta_W)^{D/2}} \exp\Big(\frac{-|\boldsymbol{\xi} - \mathbf{u}_W|^2}{2\Theta_W}\Big)$$

  with Θ_W and $\mathbf{u}_W$ the rescaled temperature and velocity imposed at the wall. Assuming that the wall does not collect particles, the "density of the wall" is given by,

  $$\int_{\boldsymbol{\xi}\in\mathbb{R}^D} \boldsymbol{\xi}\cdot\mathbf{n}(f^- + f^+)(\mathbf{x}, \boldsymbol{\xi}) d\boldsymbol{\xi} = 0 \tag{5.18}$$

- *Maxwell accommodation*
  This type of condition is a linear combination of the first two and is parametrized by $k(\mathbf{x}) \in (0,1)$ such that

$$f^-(\mathbf{x},\boldsymbol{\xi}) = k(\mathbf{x}) f^+(\mathbf{x},\mathcal{R}\boldsymbol{\xi}) + (1-k(\mathbf{x}))\mathcal{M}(\rho,\mathbf{u},\Theta)$$

  together with condition (5.18).

To get the macroscopic flux $\boldsymbol{\mathcal{J}}^{+/-}$ from the above formula, it is assumed that these conditions hold true in average if the solution of the Boltzmann equation f is replaced by the approximated distribution function $\widetilde{F}$ (3.24). This implies,

$$\int_{\boldsymbol{\xi}\cdot\mathbf{n}\leq 0} \mathbf{m}(\boldsymbol{\xi}) \otimes \boldsymbol{\xi} \Big[(\widetilde{F}^-(\mathbf{x},\boldsymbol{\xi}) - k(\mathbf{x})\widetilde{F}^+(\mathbf{x},\mathcal{R}\boldsymbol{\xi}) - (1-k(\mathbf{x}))\mathcal{M}(\rho,\mathbf{u},\Theta) \Big] d\boldsymbol{\xi} = \mathbf{0}$$

and for the "wall density" (5.18),

$$\int_{\boldsymbol{\xi}\in\mathbb{R}^D} \boldsymbol{\xi}\cdot\mathbf{n}(\widetilde{F}^+ + \widetilde{F}^-)(\mathbf{x},\boldsymbol{\xi}) d\boldsymbol{\xi} = 0$$

Hence, the incoming flux imposed at the boundary is,

$$\mathcal{J}^- = \int_{\boldsymbol{\xi}\cdot\mathbf{n}\leq 0} \mathbf{m}(\boldsymbol{\xi}) \otimes \boldsymbol{\xi} \Big[k(\mathbf{x})\widetilde{F}^+(\mathbf{x},\mathcal{R}\boldsymbol{\xi}) + (1-k(\mathbf{x}))\mathcal{M}(\rho,\mathbf{u},\Theta) \Big] d\boldsymbol{\xi}$$

With the incoming flux defined, the numerical flux at the boundary can be evaluated with the Osher-Solomon numerical flux. Remember that also the solution $\boldsymbol{U}(\boldsymbol{\lambda}^-)$ corresponding to the flux $\boldsymbol{\mathcal{J}}^-$ is needed which can be obtained by,

$$\boldsymbol{U}(\boldsymbol{\lambda}^-) = \int_{\boldsymbol{\xi}\cdot\mathbf{n}\leq 0} \mathbf{m}(\boldsymbol{\xi}) \Big[k(\mathbf{x})\widetilde{F}^+(\mathbf{x},\mathcal{R}\boldsymbol{\xi}) + (1-k(\mathbf{x}))\mathcal{M}(\rho,\mathbf{u},\Theta) \Big] d\boldsymbol{\xi} \tag{5.19}$$

The integrations over the half velocity space, which is either from 0 to ∞ or $-\infty$ to 0 are evaluated by applying the following rule,

$$\int_{-\infty}^{0} e^{-v^2} v^k dv = \frac{1}{2}\Gamma\Big(\frac{1+k}{2}\Big)(-1)^k, \qquad \int_{0}^{\infty} e^{-v^2} v^k dv = \frac{1}{2}\Gamma\Big(\frac{1+k}{2}\Big)$$

The function $\Gamma : \mathbb{R}^+ \to \mathbb{R}$ is called the complete gamma function which is defined by [17],

$$\Gamma(x) = \int_0^\infty t^{x-1} e^{-t} dt$$

5.5 Velocity space integration

The calculations of the integrals over the velocity space $\boldsymbol{\xi}$ will be performed numerically by using the Gauss-Hermite quadrature rule. This rule is related to the Gaussian quadrature rule and yield an exact solution for polynomials of degree $2n-1$ or less with n the number of integration points. It is defined by,

$$\int_{-\infty}^{+\infty} e^{-x^2} f(x) dx \approx \sum_{i=1}^{n} w_i f(x_i) \tag{5.20}$$

with x_i the integration points and w_i the corresponding weights. In the case when $F = \mathcal{M}(\rho, \mathbf{u}, \Theta)$ is a Maxwellian density or $F = \mathcal{M} \cdot \left(1 + \frac{\boldsymbol{\zeta}\cdot\mathbf{m}(\xi)}{N}\right)^N$, with $\mathcal{M}$ a local Equilibrium, the integration of $\left\langle \xi_k \mathbf{m}(\boldsymbol{\xi}) F \right\rangle$ are similar. However, the implementation for the latter can be difficult, especially for the two-dimensional case. Because only $\mathbb{R}^1$ and $\mathbb{R}^2$ spatial dimension are considered, the integration over the velocity space in the next example will be over $\mathbb{R}^2$. The integration over the one-dimensional velocity space will be similar but simpler. Suppose the following integration,

$$\left\langle \mathcal{M}\, \xi_k^{\beta 1}\, \xi_l^{\beta 2} \right\rangle = \int_{-\infty}^{+\infty} \int_{-\infty}^{+\infty} \frac{\rho}{2\pi\Theta} \exp\Big(\frac{-\|\boldsymbol{\xi} - \mathbf{u}\|_2^2}{2\Theta} \Big)\, \xi_k^{\beta 1}\, \xi_l^{\beta 2}\, d\xi_k\, d\xi_l \tag{5.21}$$

with $\beta_1, \beta_2 \geq 0$. In order to be able to apply the Gauss-Hermite rule (5.20), a change of variable needs to be done,

$$\begin{aligned} z_1^2 + z_2^2 = |\mathbf{z}|^2 &= \frac{|\boldsymbol{\xi} - \mathbf{u}|^2}{2\Theta} = \frac{(\xi_k - u_k)^2}{2\Theta} + \frac{(\xi_l - u_l)^2}{2\Theta} \\ z_1 &= \frac{\xi_k - u_k}{\sqrt{2\Theta}}, \qquad z_2 = \frac{\xi_l - u_l}{\sqrt{2\Theta}} \\ \xi_k &= \sqrt{2\Theta} z_1 + u_k, \qquad \xi_l = \sqrt{2\Theta} z_2 + u_l \end{aligned} \tag{5.22}$$

Substitute (5.22) into (5.21) to obtain,

$$\begin{aligned} &\left\langle \mathcal{M}\, \xi_k^{\beta 1}\, \xi_l^{\beta 2} \right\rangle = \\ &\frac{\rho}{2\pi\Theta} \int_{-\infty}^{+\infty} \int_{-\infty}^{+\infty} \exp(-z_1^2) \exp(-z_2^2)\, (\sqrt{2\Theta} z_1 + u_k)^{\beta 1}\, (\sqrt{2\Theta} z_2 + u_l)^{\beta 2}\, (\sqrt{2\Theta}) dz_1\, \sqrt{2\Theta} dz_2 \\ &= \frac{\rho}{\pi} \int_{-\infty}^{+\infty} \exp(-z_1^2) (\sqrt{2\Theta} z_1 + u_k)^{\beta 1} dz_1 \int_{-\infty}^{+\infty} \exp(-z_2^2) (\sqrt{2\Theta} z_2 + u_l)^{\beta 2}\, dz_2 \end{aligned} \tag{5.23}$$

Now, (5.23) has the right form to apply the Gauss-Hermite rule,

$$\left\langle \mathcal{M}\, \xi_k^{\beta 1}\, \xi_l^{\beta 2} \right\rangle \approx \frac{\rho}{\pi} \sum_{j=1}^{n} w_j (\sqrt{2\Theta} z_j + u_k)^{\beta 1} \sum_{i=1}^{n} w_i (\sqrt{2\Theta} z_i + u_l)^{\beta 2} \tag{5.24}$$

Chapter 6

Numerical simulations

This section considers the results of the numerical simulations. First, the solutions for the Euler equations versus the higher order moment systems with small Knudsen number will be presented. After that, the simulation of a rarefied gas is considered for which different order moment systems are used. Finally, a mesh convergence study will be presented. All the results are obtained for the 1 and 2 spatial dimension. The order of the basis functions are $p = 0$ for both spatial dimensions.

6.1 One-dimensional

The numerical results for the density are presented by considering the normalized density ρ_0 which is defined as,

$$\rho_0 = \frac{\rho - \rho_D}{\rho_U - \rho_D}$$

where the subscribe U denotes the upstream and D the downstream states. For the simuations in which the number of moments is higher than 3 (Euler equations), the approximated distribution function $\widetilde{F}$ uses a Maxwellian prefactor $\mathcal{M}$. This prefactor corresponds to the solution of the 3 moment systems at the final time which is in most cases $T = 0.1$.

The results presented in the sections below are obtained by the following problem setting:

- The domain of computation is $\Omega = [0, 1]$
- The initial condition consist of a Riemann problem with a left state (L) and a right state (R). The states are separated by a single discontinuity at $x = 0.5$. The values for the left and right state can be found in tables.
- Dirichlet boundary conditions are used for which the values at the left and right boundary are given by their initial conditions.

6.1.1 Euler versus higher order moment systems

As the 3 order moment system is equivalent to the Euler equations, the solutions should be identical. Also the solutions to the higher order moment systems should be similar to the

Table 6.1: Simulation properties

ρ_L	u_L	P_L	ρ_R	u_R	P_R	Kn	Δt	Δx	Time
1.0	0.0	1.0	0.5	0.0	0.4	0.0001	$0.05\times\Delta x$	1/512	0.1

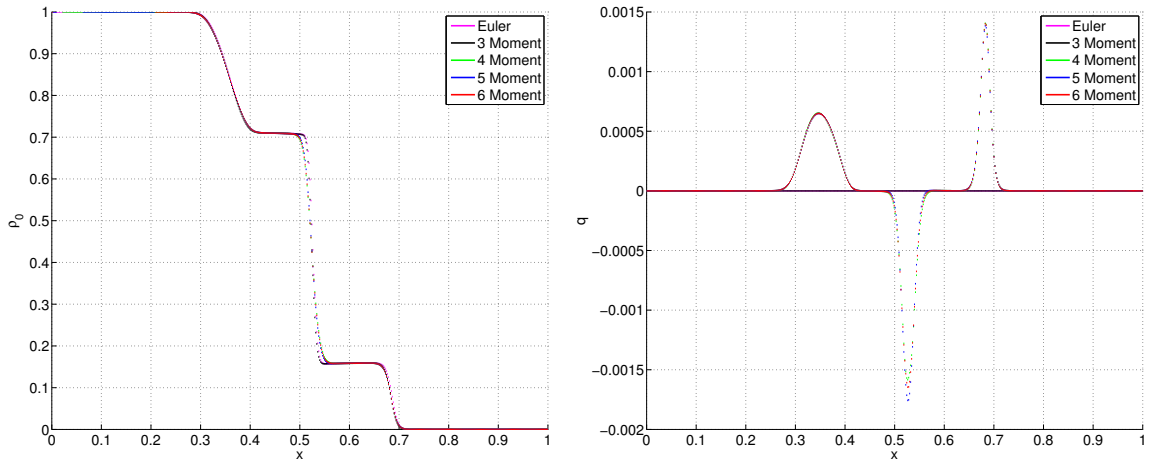

(a) Normalized density ρ_0

(b) Heat flux q

Figure 6.1: The comparison of the normalized density ρ_0 and the heat flux q between the Euler solutions and the moment systems with $Kn = 0.0001$

Euler solution when using a small Knudsen number. The results of the normalized density and heat flux are shown in figure 6.1.

Figure 6.1 depictes the solutions of the Euler equations and the moment systems. The structure of the solution of the Riemann problem for the Euler equations consists of a rarefaction wave, contact discontinuity and a shock wave [30]. The rarefaction wave consists of a continuous density, velocity and energy between the two states. For a contact discontinuity, the velocity and pressure are continuous but the density and energy discontinuous. In the case of a shock wave, all the quantities are discontinuous across the shock front. It can be observed that the solutions to the moment systems are in close agreement with the Euler equations and containing the three waves of the solution of the Riemann problem, i.e. a rarefaction wave for $0.3 < x < 0.4$, contact discontinuity in the vicinity of $x = 0.5$ and a shock wave near $x = 0.7$. Although the wave near $x = 0.7$ looks like a rarefaction wave, the velocity and energy near $x = 0.7$ are also discontinuous and thus a shock wave. Because of the small Knudsen number, the solutions of the moment systems should converge to the Euler solutions once $Kn \to 0$. Furthermore, the heat flux can not be predicted by the Euler equations and will therefore be zero. This result is also obtained by the moment systems in which the order of the predicted heat flux is 10^{-3} and thus relatively small. Observed that the region in which the moment system is not in local equilibrium is small compared to the domain of interest.

6.1.2 Transition regime

Figure 6.2 depicts the numerical results for the transition regime, lying between the continuum and free-molecular regime. The simulation properties for the Maxwellian prefactor $\mathcal{M}$ and the moment systems are the same and given in table 6.2.

Table 6.2: Simulation properties

ρ_L	u_L	P_L	ρ_R	u_R	P_R	Kn	Δt	Δx	Time
1.0	0.0	1.0	0.5	0.0	0.4	0.01	$0.05\times\Delta x$	1/512	0.1

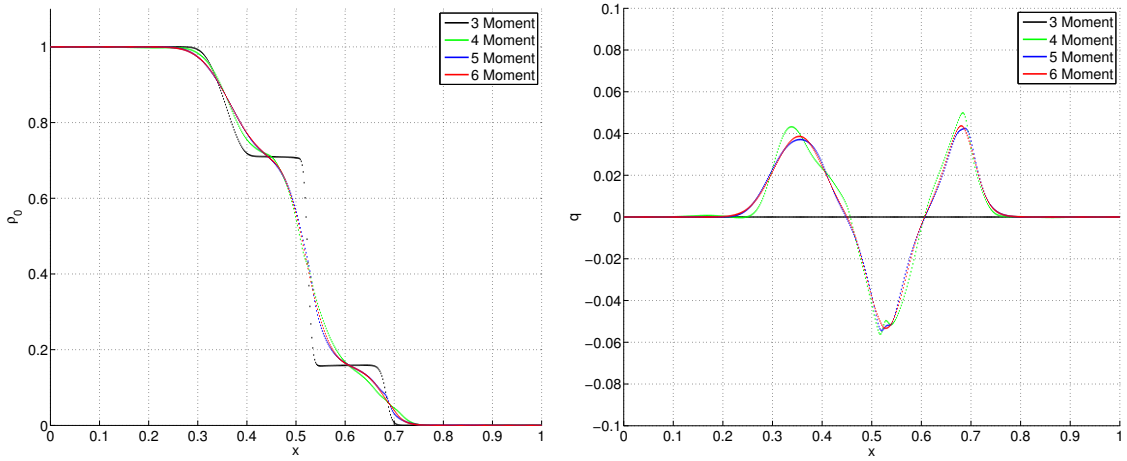

(a) Normalized density ρ_0

(b) Heat flux q

Figure 6.2: The normalized density ρ_0 and the heat flux q for a rarefied gas corresponding to $Kn = 0.01$

In the transition regime, the 3 moment system gives an identical result as the one obtained in figure 6.1 since it can only captured flows in thermodynamic equilibrium. Due to the cancellation of the collision term, there is no dependence on the Knudsen number. The solutions corresponding to the higher order moment systems are quite similar to each other but distinct from the 3 moment system. For the non-equilibrium solutions, the discontinuities appearing in the density of the 3 moment system can still be identified but are more diffuse. Therefore, the transition between the left and right initial states are smoother.

6.1.3 Modified Maxwellian prefactor

The simulations for the transition regime could only be performed with a maximum number of moments equal to 6. For higher order of moments, the Newton method used to obtain the vector of closure coefficients $\boldsymbol{\lambda}$ did not converge. After investigating the problem, it turns out that at the point x^* and time t^* where the Newton iteration did not converge, the condition number of the tangent matrix increases to the order of 10^7. Hence an error of the order 10^{-8} could not be obtained anymore.

A way to circumvent this problem is by decreasing the pressure P of the Maxwelllian prefactor $\mathcal{M}$. The condition number becomes small enough such that a numerical solution can be obtained. Figure 6.4(a) shows the Maxwellian distribution function corresponding to the different pressure values P. Figure 6.4(b) shows the condition number at the point x^* and time t^* at which the Newton method does not converge for $P = 1.0$ and does converge for $P = 0.7$. Figure 6.3 depicts the results of the normalized density and heat flux if the pressure has been change to $P = 0.7$.

By decreasing the pressure, numerical simulations including the 9 moment system can be performed. In addition, the results do look similar to the results obtained in figure 6.2 for the 3,4 and 5 moments. By even further decreasing the pressure, simulations with 9 moments and higher can be performed. This seems to be a promising step forwards. However, in order to use this result there needs to be a relation between the pressure P and for example the number of moments. This has not been found yet.

Table 6.3: Simulation properties for the Maxwellian prefactor $\mathcal{M}$

ρ_L	u_L	P_L	ρ_R	u_R	P_R	Kn	Δt	Δx	Time
1.0	0.0	0.7	0.5	0.0	0.7/2.5	0.01	$0.05\times\Delta x$	1/512	0.1

Table 6.4: Simulation properties for the higher order moment system

ρ_L	u_L	P_L	ρ_R	u_R	P_R	Kn	Δt	Δx	Time
1.0	0.0	1.0	0.5	0.0	0.4	0.01	$0.05\times\Delta x$	1/512	0.1

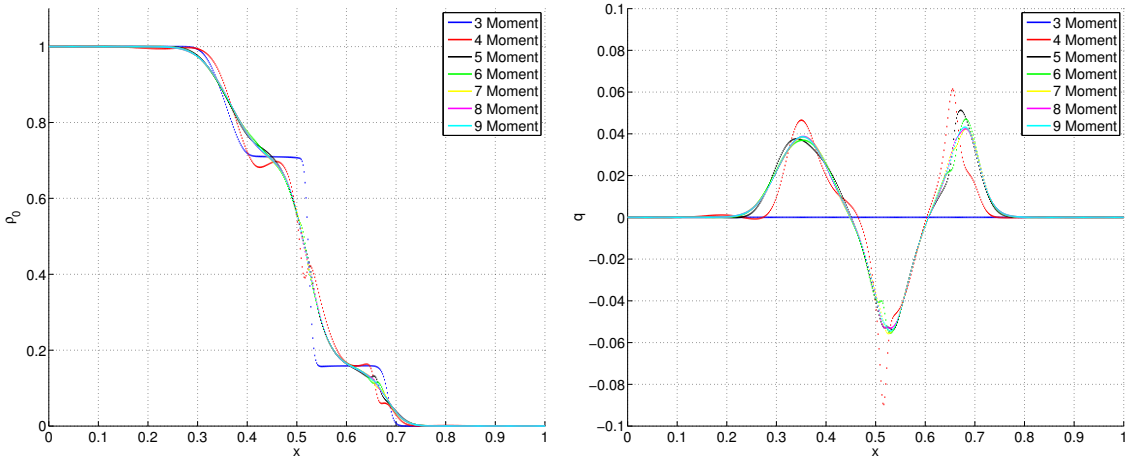

(a) Normalized density ρ_0

(b) Heat flux q

Figure 6.3: The normalized density ρ_0 and the heat flux q for a modified Maxwellian prefactor $\mathcal{M}$

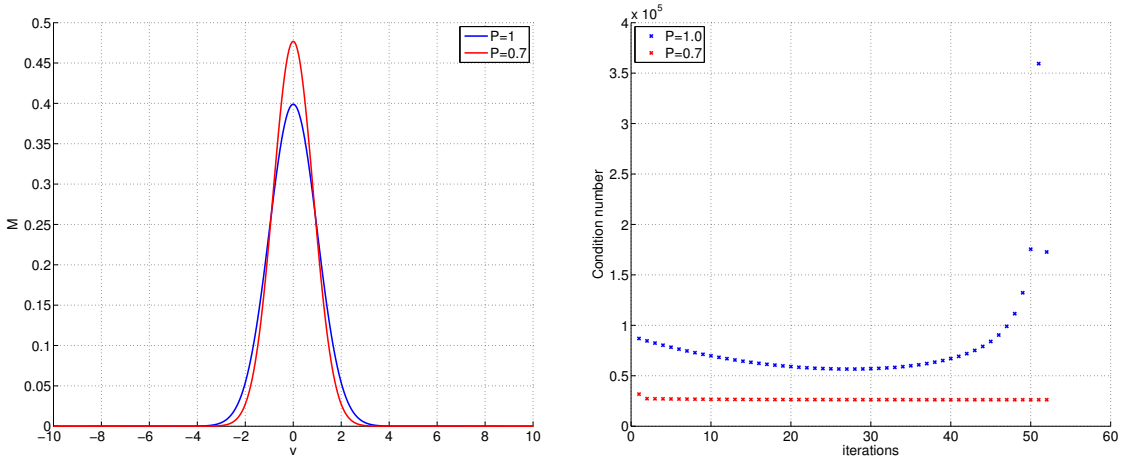

(a) Distribution function $\mathcal{M}$

(b) Condition number

Figure 6.4: The Maxwellian distribution function corresponding to $P = 1.0$ and $P = 0.7$; The condition number at the point x^* and time t^* at which the Newton method does not converge if $P = 1.0$ and does converge for $P = 0.7$

6.1.4 Mesh convergence

In order to investigate the accuracy of the numerical solutions under mesh refinements, a convergence study has been carried out. Let $\boldsymbol{u} \in \mathbb{R}^D$ and u_j its elements with $j = 1, .., D$. Then the error ϵ is defined as,

$$\varepsilon = \left(\sum_{j=1}^{D} \| u_j^h - u_j^{ref} \|^2_{L^2(\Omega)} \right)^{1/2} \tag{6.1}$$

where u^{ref} is an approximation to the exact solution which is obtained with a very dense mesh. Furthermore, the solution u_j corresponds to the solution at the final time $T = 0.05$. For the simulations, the timestep is fixed at $\Delta t = 6.25 \times 10^{-5}$, independent of the number of elements.

Table 6.5: Simulation properties

ρ_L	u_L	P_L	ρ_R	u_R	P_R	Kn	Δt	Time
1.0	0.0	1.0	0.5	0.0	0.4	0.01	6.25×10^{-5}	0.05

Continuous initial condition

The optimal convergence rate for the L^2 error is equal to $r = p + 1$ with p the order of the basis functions which is equal to zero for all the simulations. Hence the optimal rate is equal to $r = 1$. It can be observed in figure 6.5 that this is the case if a continuous initial condition is used. Even for higher order of moments, the same convergence rate is achieved. For the case of a discontinuous initial condition depicted in figure 6.6, the optimal rate is not achieved. In this case, the convergence rate tends to converge to $1/2$ for every moment system.

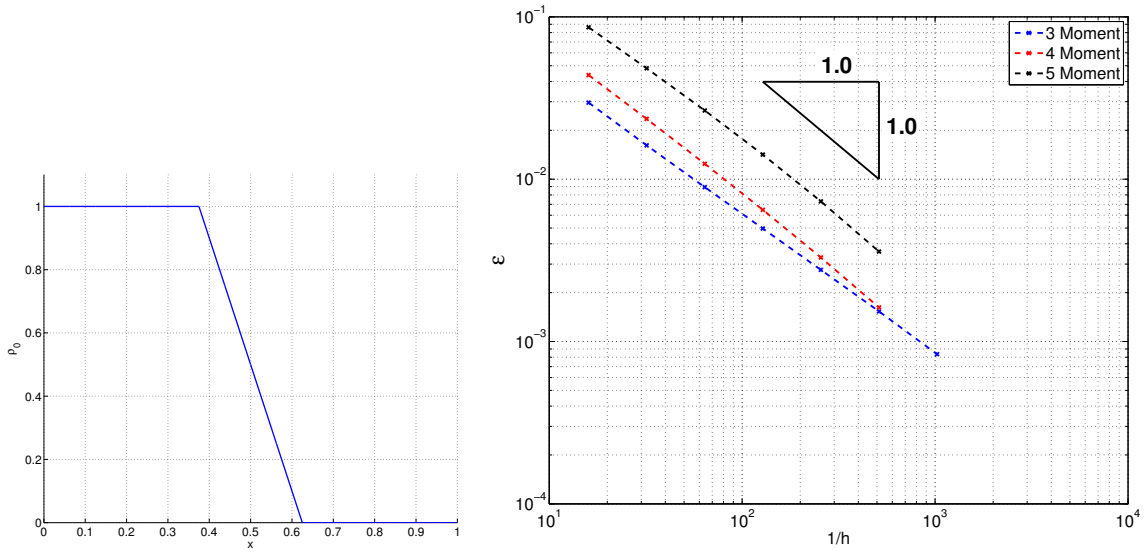

(a) Inital condition

(b) Error ε

Figure 6.5: The continuous initial condition of the normalized density ρ_0 and the error ε versus the degrees of freedom $1/h$

The reason why optimal convergence can not be achieved in the case of discontinuous initial condition can be considered as follows. Although it is more intuitive than a mathematically proof. The solutions corresponding to figure 6.5 are smooth implying that no discontinuities arise as time progresses. Thus a refinement of the mesh will make the solution even more "smooth". For the case of the discontinuous initial condition, figure 6.6, the solutions are depicted in figure 6.1. Remember that the final time in figure 6.1 is $T = 0.1$ and for the convergence test is $T = 0.05$. This implies that the solutions for the moment system 4,5 and 6 are not as smooth as depicted in figure 6.1. Because of the discontinuities they contain in their solutions, the optimal convergence rate can not be achieved.

Another observation from figure 6.6 is that the rate of convergence of the 4 and 5 moment system seems to be higher than the 3 moment system. This results from the fact that the solutions of the 4 moment system and higher produce smoother solutions as time progresses. Hence, the discontinuities will disappear and the convergence rate will converge to 1. Note that this is only the case if the error ε contains the solutions at the final time. If the error includes the solutions at every timestep, the convergence rate will remain suboptimal.

Discontinuous initial condition

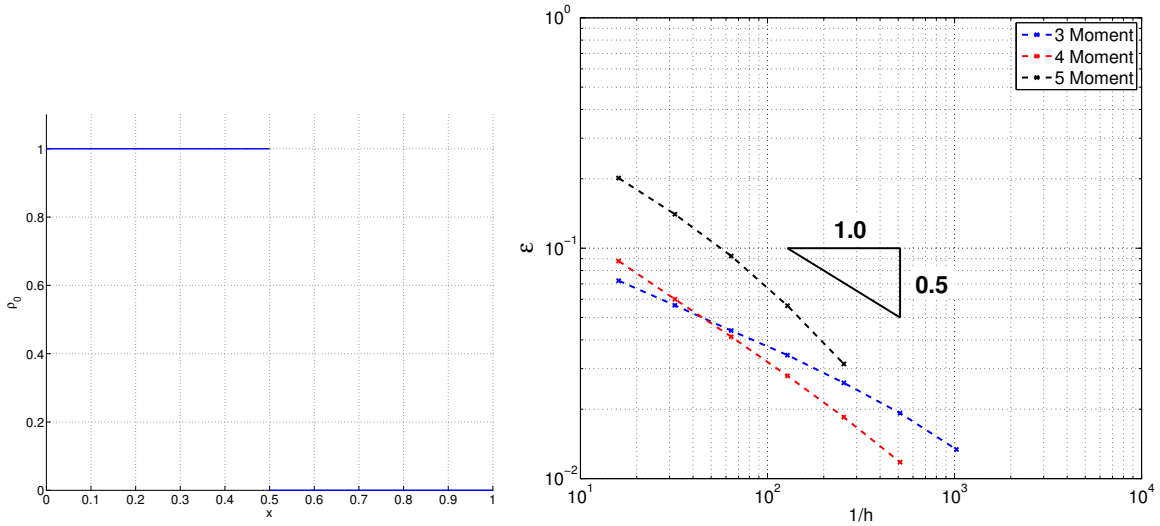

(a) Inital condition

(b) Error ε

Figure 6.6: The discontinuous initial condition of the normalized density ρ_0 and the error ε versus the degrees of freedom $1/h$

6.2 Two-dimensional

The problem setting for the 2d numerical simulations is as follows:

- The domain of computation is $\Omega = [0, 1] \times [0, 1]$
- The initial condition is composed of two constant states in two complementary regions of the domain. The inner part I is located between $0.4 < x < 0.6$ and $0.4 < y < 0.6$, the outer part O contains the rest of the domain. Their values are given in the tables.
- Dirichlet boundary conditions are used for which the values at the boundaries are given by their initial conditions

The velocity weight vectors $\boldsymbol{m}(\boldsymbol{\xi})$ used in the simulations are,

$$\boldsymbol{m}(\boldsymbol{\xi}) = \{1, \boldsymbol{\xi}, |\boldsymbol{\xi}|^2\}, \qquad \boldsymbol{m}(\boldsymbol{\xi}) = \{1, \boldsymbol{\xi}, \boldsymbol{\xi} \otimes \boldsymbol{\xi}\}$$
$$\boldsymbol{m}(\boldsymbol{\xi}) = \{1, \boldsymbol{\xi}, \boldsymbol{\xi} \otimes \boldsymbol{\xi}, \boldsymbol{\xi} \otimes \boldsymbol{\xi} \otimes \boldsymbol{\xi}\}, \qquad \boldsymbol{m}(\boldsymbol{\xi}) = \{1, \boldsymbol{\xi}, \boldsymbol{\xi} \otimes \boldsymbol{\xi}, \boldsymbol{\xi} \otimes \boldsymbol{\xi} \otimes \boldsymbol{\xi}, \boldsymbol{\xi} \otimes \boldsymbol{\xi} \otimes \boldsymbol{\xi} \otimes \boldsymbol{\xi}\}$$

6.2.1 The 4 and 6 moment systems

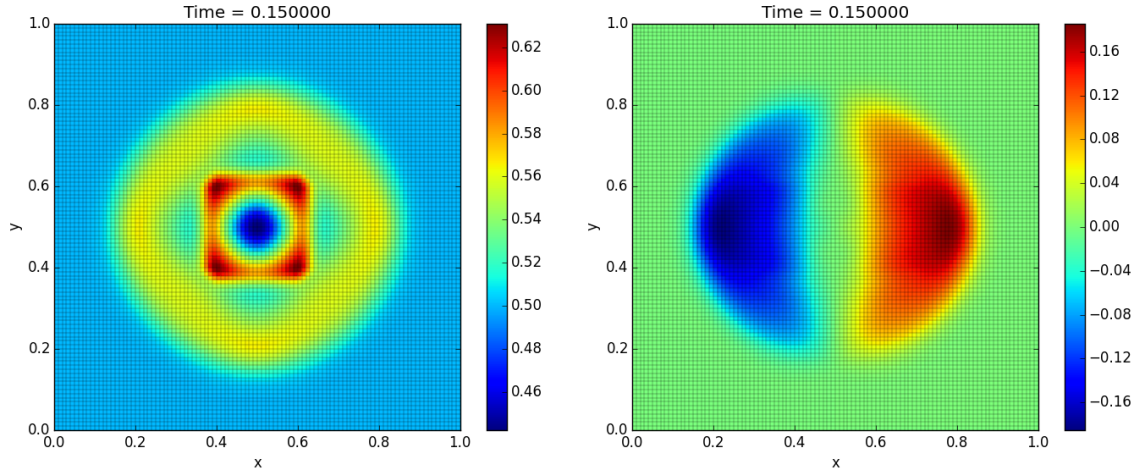

(a) Density ρ (b) Velocity u_x

Figure 6.7: The density ρ and the velocity u_x with $\boldsymbol{m} = \{1, \boldsymbol{\xi}, |\boldsymbol{\xi}|^2\}$

Table 6.6: Simulation properties

ρ_I	u_I	P_I	ρ_O	u_O	P_O	Kn	Δt	$\Delta x = \Delta y$	Time
1.0	0.0	1.0	0.5	0.0	0.4	0.01	$0.005 \times \Delta x$	1/100	0.15

Figure 6.7 depicts the results for the velocity weight vector $\boldsymbol{m}(\boldsymbol{\xi})$ which corresponds to the Euler solutions in 2d. In figure 6.8, the results for the velocity weight vector $\boldsymbol{m}(\boldsymbol{\xi}) = \{1, \boldsymbol{\xi}, \boldsymbol{\xi} \otimes \boldsymbol{\xi}\}$ are presented. The latter moment system is an extension to the Euler system. It improves upon the 4 moment system by having a non zero stress tensor. However, the heat

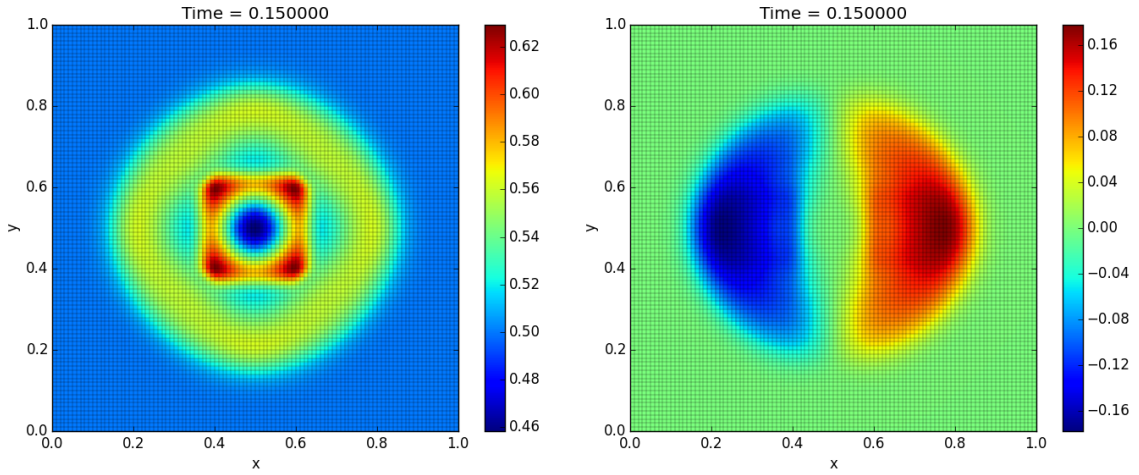

(a) Density ρ (b) Velocity u_x

Figure 6.8: The density ρ and the velocity u_x with $\boldsymbol{m} = \{1, \boldsymbol{\xi}, \boldsymbol{\xi} \otimes \boldsymbol{\xi}\}$

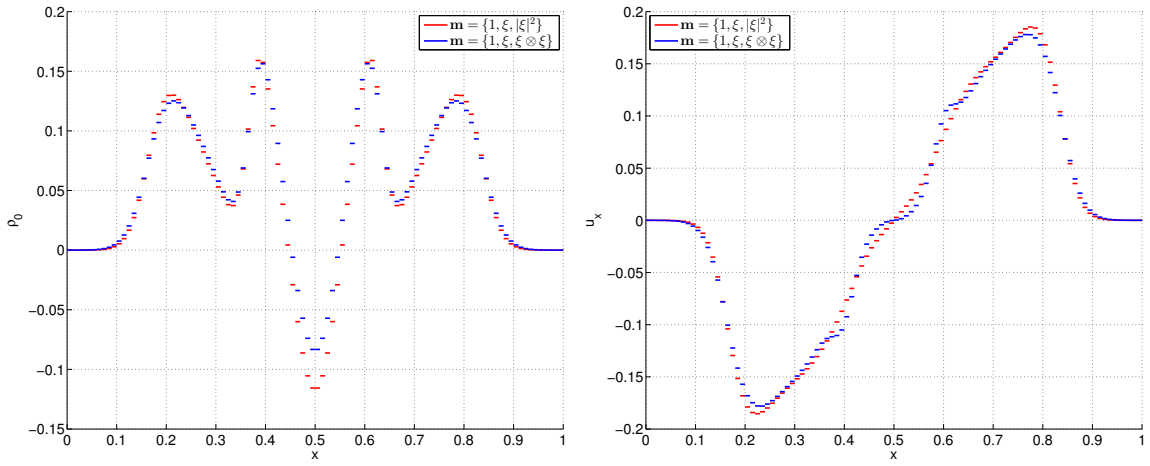

(a) Normalized density ρ_0 at $y = 0.5$ (b) Velocity u_x at $y = 0.5$

Figure 6.9: The normalized density ρ_0 and the velocity u_x at $y = 0.5$ for $\boldsymbol{m} = \{1, \boldsymbol{\xi}, |\boldsymbol{\xi}|^2\}$ and $\boldsymbol{m} = \{1, \boldsymbol{\xi}, \boldsymbol{\xi} \otimes \boldsymbol{\xi}\}$

flux will still be zero. The results for the density and velocity do have similar shapes and magnitudes. Figure 6.9 shows the normalized density ρ_0 and velocity u_x at $y = 0.5$. Also here, it can be observed that the distinction between the moment systems is small. Although, one needs to refine the mesh in order to see how similar the results are.

6.2.2 The 10 and 15 moment systems

Table 6.7: Simulation properties

ρ_I	u_I	P_I	ρ_O	u_O	P_O	Kn	Δt	$\Delta x = \Delta y$	Time
1.0	0.0	1.0	0.5	0.0	0.4	0.01	$0.0005 \times \Delta x$	1/100	0.15

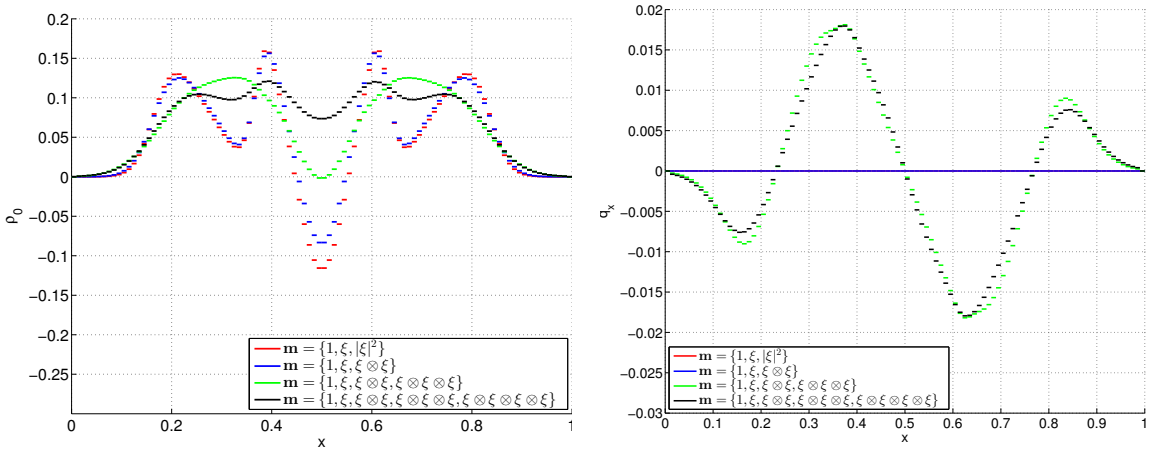

(a) The normalized density ρ_0 at $y = 0.5$ for

(b) Heat flux q_x at $y = 0.5$

Figure 6.10: The normalized density ρ_0 and the heat flux q_x at $y = 0.5$ for the 4,6,10 and 15 moment system

Figure 6.10(a) presents the normalized density for the 4,6,10 and 15 moment systems at $y = 0.5$. A quite distinction can be observed between the higher order moment systems. Especially, the density for the 10 and 15 moment systems are not comparable. This could be an indication that higher order of moments are needed to see a convergence of the density. Furthermore, a mesh refinement needs to be considered as well such that potential discontinuities can be captured.

In figure 6.12, the density ρ, velocity u_x and the heat flux q are shown for the 10 and 15 moment system in a 2d plot. Also here, the distinction in the densities is observable whereas the shape of the velocity and heat fluxes are similar. Note that the magnitudes between the moment systems are also similar.

6.2.3 Mesh-convergence

The mesh convergence has been studied for the 2D 3 moment system. The error ε is defined in (6.1).

Table 6.8: Simulation properties

ρ_I	u_I	P_I	ρ_O	u_O	P_O	Δt	Time
1.0	0.0	1.0	0.5	0.0	0.4	3.125×10^{-5}	0.01

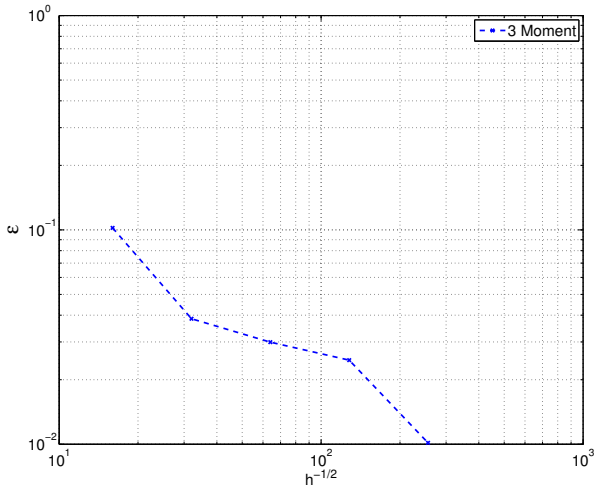

Figure 6.11: The error ε versus the degrees of freedom $1/\sqrt{h}$

The prediction of the convergence rate is rather difficult because of the small amount of refinements. As for the one-dimensional case, the optimal convergence rate will probably not be obtained due to the discontinuous initial condition. As $h \to 0$, the most relevant convergent rate will be similar to the one dimensional case which is $1/2$.

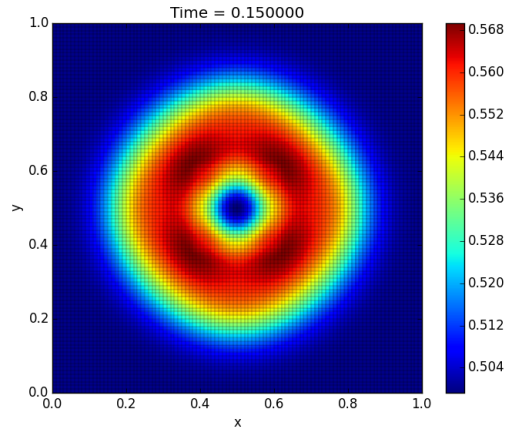

(a) Density ρ for $\boldsymbol{m} = \{1, \boldsymbol{\xi}, \boldsymbol{\xi} \otimes \boldsymbol{\xi}, \boldsymbol{\xi} \otimes \boldsymbol{\xi} \otimes \boldsymbol{\xi}\}$

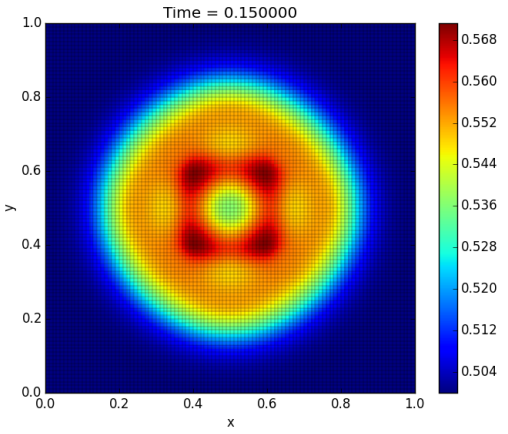

(b) Density ρ for $\boldsymbol{m} = \{1, \boldsymbol{\xi}, \boldsymbol{\xi} \otimes \boldsymbol{\xi}, \boldsymbol{\xi} \otimes \boldsymbol{\xi} \otimes \boldsymbol{\xi}, \boldsymbol{\xi} \otimes \boldsymbol{\xi} \otimes \boldsymbol{\xi} \otimes \boldsymbol{\xi}\}$

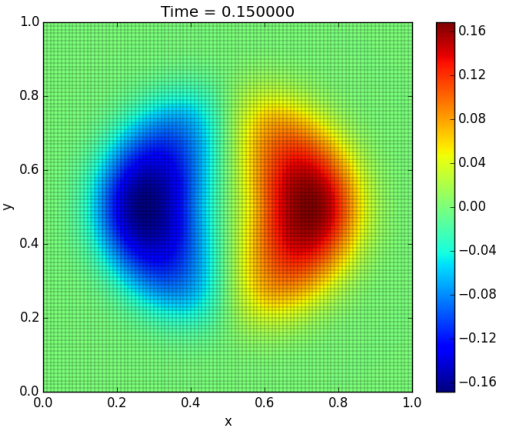

(c) Velocity u_x for $\boldsymbol{m} = \{1, \boldsymbol{\xi}, \boldsymbol{\xi} \otimes \boldsymbol{\xi}, \boldsymbol{\xi} \otimes \boldsymbol{\xi} \otimes \boldsymbol{\xi}\}$

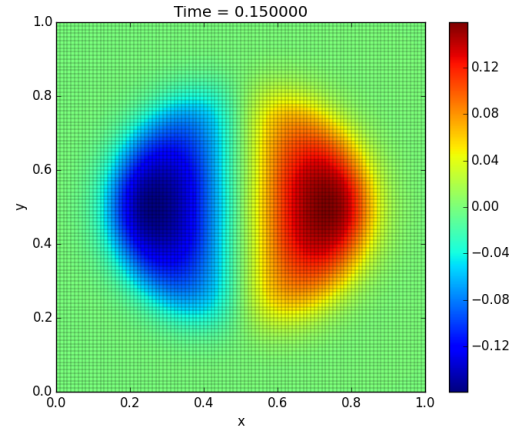

(d) Velocity u_x for $\boldsymbol{m} = \{1, \boldsymbol{\xi}, \boldsymbol{\xi} \otimes \boldsymbol{\xi}, \boldsymbol{\xi} \otimes \boldsymbol{\xi} \otimes \boldsymbol{\xi}, \boldsymbol{\xi} \otimes \boldsymbol{\xi} \otimes \boldsymbol{\xi} \otimes \boldsymbol{\xi}\}$

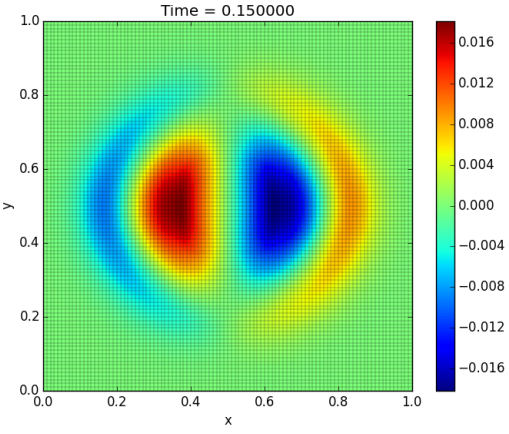

(e) Heat flux q_x for $\boldsymbol{m} = \{1, \boldsymbol{\xi}, \boldsymbol{\xi} \otimes \boldsymbol{\xi}, \boldsymbol{\xi} \otimes \boldsymbol{\xi} \otimes \boldsymbol{\xi}\}$

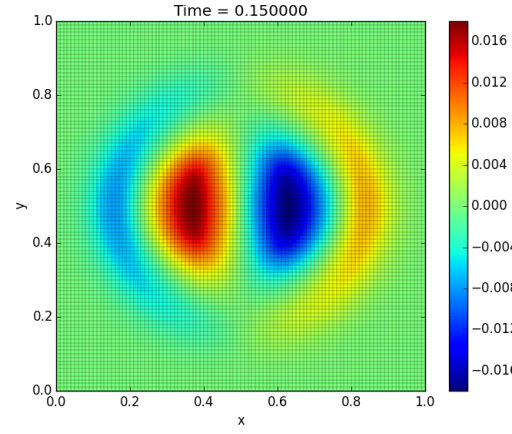

(f) Heat flux q_x for $\boldsymbol{m} = \{1, \boldsymbol{\xi}, \boldsymbol{\xi} \otimes \boldsymbol{\xi}, \boldsymbol{\xi} \otimes \boldsymbol{\xi} \otimes \boldsymbol{\xi}, \boldsymbol{\xi} \otimes \boldsymbol{\xi} \otimes \boldsymbol{\xi} \otimes \boldsymbol{\xi}\}$

Figure 6.12: The heat flux q_x for different velocity weight vectors $\boldsymbol{m}(\boldsymbol{\xi})$

Chapter 7

Conclusion and Outlook

7.1 Summary

This work is concerned with the applicability of the new class of moment closure approximations [19] into a Discontinuous Galerkin finite element method. The author in [19] has shown that the closed moment system with the new approximate entropy minimization distribution $\widetilde{F}$ still remains the fundamental properties of the Bolztmann equation. Which implies that the closed moment system is a symmetric hyperbolic system implying well-posedness, a solution to the moment system satisfy the dissipation relation (3.15) and the system retains conservation of mass, momentum and energy as well as Galilean invariance.

The original collision integral contains a complicated structure which makes the evaluation and numerical implementation difficult. Therefore, a collision model has been introduced in order to simplify the evaluation and implementation. The selected model in this work has been the BGK model. It has been shown that this model satisfies the three fundamental properties of the the original collision integral $\mathscr{C}(f)$ given in 3.1.1. Furthermore, the derivation of a relaxation time τ which depends on the Knudsen number Kn, pressure P and density ρ has been included.

The numerical approximation of the closed moment system has been considered by using a Discontinuous Galerkin finite element method. In particular, the introduction and derivation of a numerical flux needed to uniquely define integrals over the element interfaces. As well as the treatment of different boundary conditions. They are imposed by adapting the distribution function at the boundary such that one has either specular reflection, reflection with full accommodation or a combination of these two called the Maxwellian accommodation.

Finally, the results of the numerical simulations for the closed moment system in 1 and 2 spatial dimensions are presented. Results for different number of moments in both spatial dimensions are obtained. The numerical results indicate that the numerical approximations converge under moment refinement, i.e. by increasing the number of moments. The modification of the Maxwellian prefactor $\mathcal{M}$ shows the ability of obtaining numerical solutions with the number of moments higher than 6. However, there is no relation between the number of moments and the way of modifying the prefactor. Therefore, those results should be interpreted with care. The choice of the initial conditions shows an influence on the convergence rate. Continuous and "smooth" initial conditions shows an alsmost optimal convergence rate of 1 in the L^2 norm whereas for a discontinuous initial condition this optimal rate can not be achieved. It seeks to have a convergence rate of at most 1/2.

7.2 Outlook

This work has extended the new class of moment closure approximation given in [19] into a Discontinuous Galerkin finite element method. It has shown the numerical solutions for different number of moments. To be more presice, numerical solutions to the 3,4,5, and 6 moment systems were obtained in the 1d case as well as the solutions to the 4,6,10 and 15 moment systems for the 2d case. Although some promising numerical results have been obtained in 1d and 2d, there still remain other issues to investigate.

The first one is the convergence of the solution for an increasing number of moments. The more moments are included the better the distribution function will be approximated. However, one seeks to use the minimum number of moments such that the solution has been converged within a certain error. An accuracy estimate of the solution on the number of moments would therefore be very usefull.

The second one is the modification of the Maxwellian prefactor. It has been showed that modifying the pressure, numerical solutions for the 9 moment system could be obtained. However, the value for the pressure needs to be prescibed. This could be done by finding a relation with the number of moments for example. A maybe more important point is the influence of adapting the pressure on the accuracy of the solutions.

Another issue is the mesh sensitivity of the 2d numerical simulations. The results presented in the previous chapter where obtained with a relatively coarse mesh of 100×100 elements. Because the accuracy of the solutions increases if more elements are used, a study on how mesh sensitivity is related to solvability of the problem would be very usefull.

In the context of gas flows in transition regimes, an increase of the Knudsen number should be considered. Also here, the solvability of the problem is related to the Knudsen number. A further investigation on this sensitivity will be necessary. One could considered a different collision model instead of the BGK model.

Finally, incorporating the boundary conditions will improve the applicability of the numerical simulations. Especially, rarefied gas flow interaction with the wall can be considered.

Bibliography

[1] Pierre Andries, Jean-François Bourgat, Patrick Le Tallec, and Benoît Perthame. Numerical comparison between the Boltzmann and ES-BGK models for rarefied gases. Research Report RR-3872, 2000. Projet M3N.

[2] T. Barth. On discontinuous galerkin approximations of boltzmann moment closure with levermore closure. *Computer Methods in Applied Mechanics and Engineering*, 195:3311–3330, 2006.

[3] G.A. Bird. Definition of mean free path for real gases. *Physics of Fluids (1958-1988)*, 26(11):3222–3223, 1983.

[4] G.A. Bird. *Molecular Gas Dynamics and the Direct Simulation of Gas Flows*. Oxford Engineering Science Series; 42. Clarendon Press, Oxford, 1994.

[5] Z. Cai and R. Li. Numerical regularized moment method of arbitrary order for boltzmann-bgk equation. pages 1–33, 2010. `http://arxiv.org/pdf/1002.2021v3.pdf`.

[6] M.J. Castro, J.M. Gallardo, and A. Marquina. Approximate osher-solomon schemes for hyperbolic systems. *Applied Mathematics and Computation*, 2015.

[7] C. Cercignani. *The Boltzmann Equation and Its Applications*, volume 67 of *Applied Mathematical Sciences*. Springer, New York, 1988.

[8] C. Cercignani. *Rarefied Gas Dynamics: From Basic Concepts to Actual Calculations*. Cambridge Texts in Applied Mathematics (Book 21). Cambridge University Press, 1th edition, 2000.

[9] C. Cercignani and Centro Internazionale Matematico Estivo. *Kinetic Theories and the Boltzmann Equation: Lectures Given at the 1st 1981 Session of the Centro Internazionale Matematico Estivo (C.I.M.E.), Held at Montecatini, Italy, June 10-18, 1981*. Springer-Verlag.

[10] C. Cercignani, R. Illner, and M. Pulvirenti. *The Mathematical Theory of Dilute Gases*, volume 106 of *Applied Mathematical Sciences*. Springer, New York, 1994.

[11] C.Shen. *Rarefied Gas Dynamics: Fundamentals, Simulations and Micro Flows*. Springer-Verlag Berlin Heidelberg, 1th edition, 2005.

[12] L. Desvillettes. Some applications of the method of moments for the homogeneous boltzmann and kac equations. *Archive for Rational Mechanics and Analysis*, 123(4):387–404, 1993.

[13] M. Dumbser and E.F. Toro. On universal osher-type schemes for general nonlinear hyperbolic conservation laws. *Communications in Computational Physics*, 10(3):635–671, 2011.

[14] H. Grad. On the kinetic theory of rarefied gases. *Communications on Pure and Applied Mathematics*, 2:331–407, 1949.

[15] C.D. Hauck. *Entropy-Based Moment Closure in Semiconductor Models.* PhD thesis, University of Maryland, College Park, 2006.

[16] P.W. Hemker and S.P. Spekreijse. Multigrid solution of the steady euler equations. In D. Braess, W. Hackbusch, and U. Trottenberg, editors, *Advances in Multi-Grid Methods*, volume 11, December 1985.

[17] E. Kreyszig. *Advanced Engineering Mathematics.* John Wiley and Sons, 8th edition, 1999.

[18] C.D. Levermore. Moment closure hierarchies for kinetic theories. *Journal of Statistical Physics*, 83:1021–1065, 1996.

[19] M.R.A. Abdel Malik and E.H. van Brummelen. Numerical approximation of the boltzmann equation: Moment closure. Master's thesis, Technical University Eindhoven University of Technology, September 2012.

[20] J. McDonald and M. Torrilhon. Robust hyperbolic moment closures for cfd. In M. Mareschal and A. Santos, editors, *American Institute of Physics Conference Series*, volume 1501 of *American Institute of Physics Conference Series*, pages 191–198, November 2012.

[21] J.G. McDonald. *Extended Fluid-Dynamic Modelling for Numerical Solution of Micro-Scale Flows.* PhD thesis, University of Toronto, 2011.

[22] J.G. McDonald and C.P.T. Groth. Towards physically realizable and hyperbolic moment closures for kinetic theory. *Continuum Mechanics and Thermodynamics*, 21:467–493, 2009.

[23] J.G. McDonald and C.P.T. Groth. Towards realizable hyperbolic moment closures for viscous heat-conducting gas flows based on a maximum-entropy distribution. *Continuum Mechanics and Thermodynamics*, 25:573–603, 2013.

[24] L. Mieussens and H. Struchtrup. Numerical comparison of bhatnagar-gross-krook models with proper prandtl number. *Physics of Fluids*, 16:2797–2813, aug 2004.

[25] P.L.Bhatnagar, E.P.Gross, and M.Krook. A model for collision processes in gases. *Physical Review Letters*, 94(3):511, 1954.

[26] H. Struchtrup. The bgk model with velocity-dependent collision frequency. *Continuum Mechanics and Thermodynamics*, 9:23–31, February 1997.

[27] H. Struchtrup. *Macroscopic Transport Equations for Rarefied Gas Flows: Approximation Methods in Kinetic Theory*. Interaction of Mechanics and Mathematics. Springer Berlin Heidelberg, 2005.

[28] P. Le Tallec and J.P. Perlat. Numerical analysis of levermore's moment system. Research report 3124, Institut National de Recherche en Informatique et en Automatique (INRIA), March 1997. Project M3N.

[29] P. Le Tallec and J.P. Perlat. Boundary conditions and existence results for levermore's moments system. *Mathematical Models and Methods in Applied Sciences*, 10(1):127–152, 2000.

[30] E.F. Toro. *Riemann Solvers and Numerical Methods for Fluid Dynamics: A Practical Introduction*. Springer Berlin Heidelberg, 2009.

[31] W.G. Vincenti and Jr C.H. Kruger. *Introduction to Physical Gas Dynamics*. Krieger, 1986.